

Current Research in Microbiology

Chapter 6

Stability, Flexibility, and Function of Dihydrofolate Reductases from *Escherichia coli* and Deep-Sea Bacteria

Ohmae E¹*; Gekko K^{1,2}

¹Department of Mathematical and Life Sciences, Graduate School of Science, Hiroshima University, Higashi-Hiroshima, Hiroshima 739-8526, Japan.

²Hiroshima Synchrotron Radiation Center, Hiroshima University, Higashi-Hiroshima, Hiroshima 739-0046, Japan.

*Correspondence to: Ohmae E, Department of Mathematical and Life Sciences, Graduate School of Science, Hiroshima University, Higashi-Hiroshima, Hiroshima 739-8526, Japan.

Email: ohmae@hiroshima-u.ac.jp

Abstract Dihydrofolate reductase (DHFR) is an important target for investigating the linkage between structural flexibility and catalytic function because it is a ubiquitous enzyme existing in all organisms. Site-directed substitution or deletion in flexible loops of *Escherichia coli* DHFR significantly affects the stability, flexibility, and catalytic function, although distal residues have not been recognized as dynamically and functionally significant. Nonadditive effects of double substitution or deletion in different loops demonstrate the existence of long-range coupling between the loop motions that include other distal residues. Compressibility changes due to loop substitutions and ligand binding reveal that the modified flexibility and function can be mainly attributed to changes in internal cavities or atomic packing. DHFRs from deep-sea bacteria exhibit species-specific pressure-dependence on stability and function that provide useful information on the roles of structural flexibility in molecular adaptation to high-pressure environments. These findings give new insight into the structure–flexibility–function relationship of DHFR.

Abbreviations: cAMP: cyclic adenosine monophosphate; CD: circular dichroism; DHF: dihydrofolate; DHFR: dihydrofolate reductase; H/D: hydrogen to deuterium; IPMDH: 3-isopropylmalate dehydrogenase; MD: molecular dynamics; MS: mass spectrometry; MTX: methotrexate; NADPH: reduced nicotinamide adenine dinucleotide phosphate; NADP⁺: oxidized nicotinamide adenine dinucleotide phosphate; NMR: nuclear magnetic resonance; THF: tetrahydrofolate; TOF: time of flight

1. Introduction

Dihydrofolate reductase (DHFR) is an important enzyme that exists ubiquitously in all organisms. DHFR catalyzes the reduction of dihydrofolate (DHF) to tetrahydrofolate (THF) by utilizing the reducing cofactor NADPH (reduced nicotinamide adenine dinucleotide phosphate). THF and its derivatives are essential for the syntheses of purine and thymine bases of DNA, and hence DHFR plays a central role in cell growth and proliferation. DHFR is also a clinically important enzyme not only as the target of several antifolate drugs, such as trimethoprim and methotrexate (MTX), but also as an enzyme for producing *l*-leucovorin, an anticancer drug, in a stereospecific manner.

DHFRs from various organisms living in normal and extreme environments have been investigated on the basis of the sequence conservation, backbone flexibility, and enzyme kinetics [1–4]. Among them, DHFR from *Escherichia coli* (ecDHFR) is the most widely investigated because it is a suitable target for investigating the linkage between protein dynamics and catalytic function. The catalytic reaction of ecDHFR is known to occur along a preferred reaction pathway involving several intermediate states that include hydride transfer [5]. The important role of structural dynamics in function of this enzyme was indicated on the basis of various dynamics and catalytic data [6,7]. Sawaya and Kraut [8] proposed a dynamic model for conformational changes during the catalytic cycle based on crystal structures of ecDHFR–ligand complexes analogous to the kinetics intermediates. Studies of mutations within or in the vicinity of the active site [9–14] have uncovered the roles of the residues around the active site, but the roles of those distant from the active site have remained unclear.

The participation of distal residues in catalytic function was demonstrated using various site-directed mutations [15,16], with subsequent studies showing motional couplings between the residues in the active site and the distal residues, which preorganize the Michaelis complex for catalysis [7,17]. A computational simulation showed that the effect of a distal mutation may propagate to active-site residues through modulation of the correlated motion [18]. Although these studies have indicated the significance of distal residues, the relationship between structural flexibility and catalytic function remains controversial because the active-site fluctuation is mediated in a complicated manner by a motional hierarchy of the entire protein molecule, including thermal fluctuation of individual amino acid residues, loop motions, and reorientation of structural domains.

There have also been many studies of DHFRs from microorganisms living in extreme environments of temperature, pressure, salt concentration, pH, etc. in relation to molecular evolution and pharmaceutical applications: hyperthermophilic bacterium *Thermotoga maritima* [19–21], psychrophilic and piezophilic bacterium *Moritella profunda* [22–24], extremely halophilic bacteria *Haloferax volcanii* [25–27] and *Haloarcula japonica* [28,29], and alka-

lipophilic bacterium *Bacillus halodurans* [30]. These studies have revealed characteristic species-dependent structures and functions of DHFR, but the molecular mechanisms underlying the adaptation to particular environmental conditions remain unclear. Among these extreme environments, the deep sea is of special interest because the various piezophilic, piezosensitive, and piezotolerant species that live there exhibit characteristics that vary with the depth (i.e., hydrostatic pressure).

While conducting such studies of DHFR, we have systematically investigated the effects of loop mutation of ecDHFR and the species dependence of deep-sea DHFRs on stability, flexibility, and function, based on the hypothesis that the atomic packing plays an important role in the overall fluctuation relevant to catalytic function. In 1993 we found that mutations at Gly121 in a loop distant from the active site of ecDHFR affect the stability and function, and proposed that the effects of loop mutation could extend to the entire protein molecule [31]. The subsequent investigations of loop mutations have revealed important roles of loop regions in the dynamics and function of this enzyme [32–36]. Related to the structure–flexibility–function relationship, we have also examined the effects of pressure on the stability and function of DHFRs obtained from various deep-sea bacteria [37–40]. The species-dependent pressure susceptibility of stability and function has provided useful information on the structural flexibility and the molecular adaptation of deep-sea DHFRs to extreme pressure conditions.

The present review focuses on surveying the effects of loop mutations in ecDHFR and the species dependence of deep-sea DHFRs on stability, flexibility, and function, primarily based on our experimental works. These data in combination with molecular dynamics information will deepen our understanding in the structure–flexibility–function relationship and pressure-adaptation mechanism of DHFR, which is complementary to more comprehensive reviews on the related topics [6,7,41–46].

2. Stability, Flexibility, and Function of Loop Mutants of ecDHFR

ecDHFR is a monomeric protein of 159 amino acid residues with no prosthetic group or disulfide bond. **Figure 1** shows the three-dimensional structure of the DHFR–folate–NADP⁺ (oxidized nicotinamide adenine dinucleotide phosphate) complex in crystal form [8]. It consists of eight β -strands and four α -helices, one of which includes the active site Asp27. The large B-factors suggest the appearance of five flexible loops in DHFR: Met20 (residues 9–23), α C– β C (residues 51–57), β C– β D (residues 64–72), β F– β G (residues 117–131), and β G– β H (residues 142–149) [47]. Nuclear magnetic resonance (NMR) spin relaxation analysis of the ¹⁵N-labeled DHFR–folate complex has also revealed four distinctive flexible regions: residues 16–22 in the Met20 loop, residues 67–69 in the β C– β D loop, residues 38 and 88 in the hinge region between the adenosine-binding domain (residues 38–88) and the major domain (residues 1–37 and 89–159), and residues 119–123 in the β F– β G loop [48]. The Met20 loop contacts NADPH

in a closed conformation that is stabilized by hydrogen bonding of Gly15 and Glu17 in the Met20 loop, with Asp122 in the β F– β G loop. A conformational change of the Met20 loop accompanies disruption of these hydrogen bonds to form new ones between Asn23 (Met20 loop) and Ser148 (β G– β H loop). The rearrangement of the hydrogen bond changes the Met20 loop from a closed conformation to the occluded conformation found in the product complex.

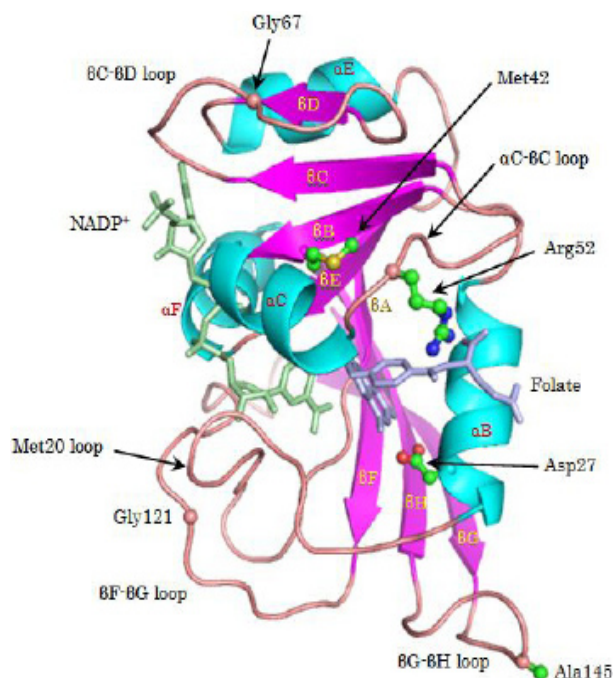


Figure 1: Crystal structure of ecDHFR in a complex with folate and NADP⁺ (PDB: 1RX2), which represents the Michaelis-complex structure [8]. Residues Met42, Arg52, Gly67, Gly121, and Ala145, which were the mutation targets in this study, and the active-site residue, Asp27, are shown by balls and sticks. The figure was drawn using the program PyMol (<http://www.pymol.org/>).

The kinetics scheme of the catalytic reaction of ecDHFR has been clarified by Benkovic and coworkers [5,12,49]. As shown in **Figure 2**, ecDHFR catalyzes the reduction of DHF to THF with the aid of coenzyme NADPH *via* five intermediates: DHFR·NADPH, DHFR·NADPH·DHF, DHFR·NADP⁺·THF, DHFR·THF, and DHFR·NADPH·THF. The rate-determining step at neutral pH is the release of the product (THF) from the reduced ternary complex (DHFR·NADPH·THF). Hydride transfer from NADPH to DHF is the key reaction step that is thought to be regulated by protein motion, the steps of which presumably require kinetically significant conformational changes to occur in the Met20 loop that comes into contact with NADPH prior to catalysis. This enzyme reaction is strongly inhibited by MTX, which is used as an anticancer drug.

A large amount of structural dynamics and catalytic data [8,16–18,48,50–61] including computational simulation [18,51,54,55,57,58,62] have provided a detailed context for the role of dynamics in function of ecDHFR. In this subject, mutation studies in the distal residues [11,15,16,50] in addition to the vicinity of the active site [9,10,12–14] have played important roles in elucidating the motional couplings between the residues in the active site and the distal

residues. Singh et al. experimentally showed the presence of a global dynamic network of coupled motions including residues 42, 121, and 133 correlated to hydride transfer [60]. An NMR study showed the participation of residue 42 in solution dynamics [63]. However, the target residues for mutation are limited and further detailed mutation studies are required for deeper understanding of the precise roles of distal residues or loops in dynamics and function.

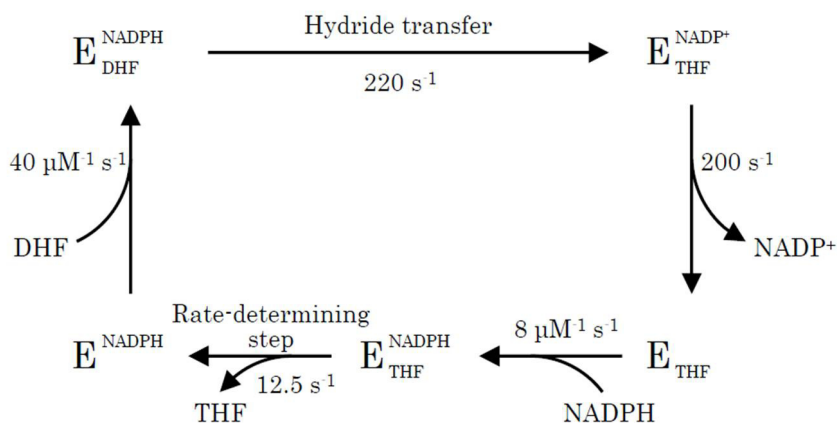


Figure 2: The catalytic cycle of ecDHFR. The five primary intermediates and the rate constants for forward reactions at pH 7 [5,50] are shown. E, dihydrofolate reductase; DHF, dihydrofolate; THF, tetrahydrofolate; NADPH, reduced nicotinamide adenine dinucleotide phosphate; NADP⁺, oxidized nicotinamide adenine dinucleotide phosphate.

We have systematically investigated the effects of loop mutation of ecDHFR on stability, flexibility, and function to demonstrate the relevance of the flexible loops to catalytic function *via* the participation in overall fluctuation [31–36]. Since the Met20 loop directly contacting NADPH is well characterized, roles of the other four loops (α C– β C, β C– β D, β F– β G, and β G– β H) have been studied using site-directed amino acid substitution or deletion around the most-flexible residues in each loop (Arg52, Gly67, Gly121, and Ala145), which are highly conserved among many DHFR sequences [31–34]. The mutation effects of another pivotal distal residue Met42 were also studied for comparison, because this residue is in the structural core that includes tightly conserved regions (residues 40–43) that do not appear to play any obvious functional roles in the crystal structure [64].

2.1. Effects of loop mutations on stability

The structural stability is evaluated by the difference in the Gibbs free energy between native and denatured states (ΔG_u°) when the denaturant (urea or guanidine hydrochloride) is at an infinite dilution:

$$\Delta G_u = \Delta G_u^\circ - m [\text{denaturant}] \quad (1)$$

where ΔG_u is the change in free energy due to denaturation at a given denaturant concentration, and coefficient m is the cooperativity parameter of the transition, which is dominantly attributable to the difference in the solvent-exposed surface area of a protein molecule between the

native and denatured states [65–67]. C_m is the denaturant concentration at the midpoint of the transition (i.e., $\Delta G_u = 0$).

2.1.1. Loop-residue substitution

The ΔG_u° , m , and C_m values for urea denaturation of substitution mutants at residues 67, 121, and 145 are listed in **Table 1** [32–34]. It is evident that the ΔG_u° values of any mutants differ from that of the wild type: ΔG_u° decreased for most mutants at residues 67 and 121 whereas it increased for most mutants at residue 145, indicating that the loops contribute to the stability in different ways. The m value was also dependent on the mutations at any residues. The ΔG_u° value increased with the m value, with correlation coefficients (r values) of 0.80, 0.72, and 0.97 for residues 67, 121, and 145, respectively. This indicates that the stability increases with the cooperativity of the transitions or the compactness of the native state.

A particularly interesting observation was that the ΔG_u° value decreased as the hydrophobicity of the introduced amino acid side chains increased. Such a reverse hydrophobic effect could be due to the denatured state being stabilized and/or the native state being destabilized by the hydrophobic interaction. The former mechanism would dominate for a mutation at residue 145, which is highly exposed to the solvent, whereas the latter would dominate for mutations at residues 67 and 121, because the ΔG_u° value decreased as the volume of the amino acid side chain introduced into both residues increased: the bulky side chain would affect the atomic packing to overcome the hydrophobic stabilization effect. In contrast to the loop mutations, the ΔG_u° values of Met42 mutants (which are also listed in **Table 1**) increased with the side-chain hydrophobicity [64]. This inverted correlation seems reasonable because Met42 is located in the hydrophobic core of the structure. The results that the stability is affected by only a single amino acid substitution in loops or distal residues suggest that the effects of the mutation extend over a long distance and so can modify the structural flexibility.

Double-mutation analyses are useful for exploring the possible couplings between distant loops [68]. The ΔG_u° values of eight double-substitution mutants at residues 67 and 121 (G67V/G121S, G67V/G121A, G67V/G121C, G67V/G121D, G67V/G121V, G67V/G121H, G67V/G121L, and G67V/G121Y) are listed in **Table 1** in comparison with those of the corresponding single substitution mutants [35]. The ΔG_u° values of these double mutants (with the exception of G67V/G121H) did not equal the sum of those of the respective single mutants (**Figure 3**). This nonadditivity represents evidence of the presence of long-range interactions between residues 67 and 121, whose α -carbons are separated by 27.7 Å. Thus, the effects of mutation at residue 67 reach residue 121, and *vice versa*. A small alteration in atomic packing due to a mutation at each site would be cooperatively magnified through motional coupling of the loops and thereby affect the structural stability.

Table 1: Thermodynamic parameters for urea denaturation (ΔG_u° , C_m , and m), partial specific volume (v°), compressibility (β_s°), and steady-state kinetics parameters (K_m and k_{cat}) of the wild-type and site-directed substitution/deletion mutants of ecDHFR^a.

DHFR	ΔG_u° (kcal mol ⁻¹)	C_m (M)	m (kcal mol ⁻¹ M ⁻¹)	v° (cm ³ g ⁻¹)	β_s° (Mbar ⁻¹)	K_m (μ M)	k_{cat} (s ⁻¹)
Wild-type	6.08±0.18	3.11	1.96±0.06	0.723±0.001	1.7±0.3	1.3±0.1	24.6±3.1
M42E	3.07±0.28	1.57	1.96±0.15	ND	ND	6.0±0.7	15.9±0.4
M42S	4.50±0.29	2.42	1.86±0.11	ND	ND	2.3±0.2	22.6±0.6
M42Q	4.37±0.22	2.12	2.06±0.10	ND	ND	2.3±0.2	24.3±0.8
M42G	4.40±0.50	1.93	2.28±0.24	ND	ND	1.2±0.1	13.0±0.4
M42T	2.90±0.39	1.90	1.53±0.17	ND	ND	0.8±0.1	18.7±0.4
M42A	5.75±0.54	2.35	2.45±0.22	ND	ND	1.3±0.2	14.0±0.8
M42H	3.06±0.43	1.57	1.95±0.22	ND	ND	1.9±0.3	26.6±1.5
M42P	4.78±1.10	3.27	1.46±0.36	ND	ND	0.8±0.1	24.0±1.1
M42C	4.81±0.26	2.29	2.10±0.11	ND	ND	1.9±0.2	30.4±1.2
M42V	5.04±0.38	2.41	2.09±0.15	ND	ND	0.9±0.1	15.7±0.7
M42L	5.34±0.51	2.52	2.12±0.19	ND	ND	1.1±0.1	18.9±0.6
M42I	5.85±0.58	2.70	2.17±0.21	ND	ND	0.6±0.1	12.4±0.5
M42Y	6.40±0.48	2.51	2.55±0.18	ND	ND	1.8±0.2	45.5±1.3
M42W	4.17±0.40	2.88	1.45±0.14	ND	ND	45.0±2.6	104.6±2.3
G67S	6.15±0.18	2.82	2.18±0.06	0.723±0.003	1.9±0.8	1.4±0.1	26.4±1.3
G67A	6.60±0.08	2.82	2.34±0.03	0.721±0.002	-0.1±0.9	1.1±0.1	20.0±0.7
G67C	5.72±0.12	2.79	2.05±0.04	0.724±0.001	1.7±0.3	1.2±0.1	24.6±3.6
G67D	5.94±0.12	2.62	2.27±0.04	0.724±0.003	3.0±0.7	1.2±0.2	20.6±2.5
G67V	5.14±0.17	2.89	1.78±0.05	0.721±0.003	1.1±0.5	1.3±0.5	19.1±1.7
G67L	5.64±0.17	2.83	1.99±0.06	0.721±0.003	-0.6±1.4	1.1±0.1	22.6±3.7
G67T	5.87±0.05	2.62	2.24±0.05	0.718±0.002	1.4±1.5	1.8±0.4	26.6±3.1
G121S	6.09±0.16	3.03	2.01±0.05	0.721±0.002	0.7±1.0	1.8	5.2
G121A	6.58±0.17	2.86	2.30±0.06	0.710±0.003	-0.4±0.4	2.7	8.5
G121C	6.17±0.22	2.86	2.16±0.07	0.725±0.001	5.5±0.5	1.5	8.4
G121D	6.27±0.15	2.70	2.32±0.03	ND	ND	1.6	0.67
G121V	5.09±0.20	2.65	1.92±0.08	0.733±0.003	3.7±2.6	1.4	0.94
G121L	5.45±0.17	2.78	1.96±0.06	ND	ND	2.3	0.94
G121H	5.97±0.23	2.64	2.26±0.09	0.713±0.002	-1.8±0.5	2.2	4.8
G121Y	5.88±0.18	2.72	2.16±0.06	0.724±0.001	-0.7±0.6	2.5	4.4
A145G	7.38±0.22	3.05	2.42±0.07	0.726±0.001	3.1±0.2	1.2±0.1	21.1±2.4
A145S	7.28±0.26	3.05	2.38±0.09	0.729±0.002	3.1±0.8	0.8±0.0	19.3±0.5
A145T	9.13±0.26	3.10	2.95±0.08	0.729±0.001	3.0±0.3	1.6±0.1	20.0±0.1
A145V	6.45±0.20	2.85	2.27±0.07	ND	ND	1.1±0.2	15.2±1.5

A145H	7.25±0.21	2.97	2.44±0.07	0.728±0.001	3.8±0.6	0.7±0.2	18.8±0.8
A145F	5.94±0.17	2.96	2.01±0.06	ND	ND	1.2±0.3	27.6±7.9
A145R	8.05±0.23	3.26	2.48±0.07	0.725±0.002	0.8±0.1	1.4±0.2	19.9±1.5
G67V/ G121S	5.86±0.14	2.72	2.15±0.05	ND	ND	2.1±0.6	1.1±0.1
G67V/ G121A	6.73±0.14	3.36	2.00±0.04	ND	ND	1.1±0.3	3.5±0.2
G67V/ G121C	4.78±0.13	2.69	1.77±0.04	ND	ND	2.0±0.5	1.5±0.1
G67V/ G121D	4.77±0.13	2.50	1.91±0.05	ND	ND	2.4±1.0	0.3±0.1
G67V/ G121V	5.15±0.10	2.51	2.05±0.04	ND	ND	3.3±0.7	0.7±0.1
G67V/ G121H	5.05±0.13	2.51	2.01±0.05	ND	ND	1.4±0.7	1.6±0.3
G67V/ G121L	5.07±0.14	2.73	1.85±0.05	ND	ND	2.0±0.9	2.0±0.3
G67V/ G121Y	7.08±0.17	3.24	2.19±0.06	ND	ND	2.6±0.8	1.0±0.1
Δ52	6.52±0.40	3.24±0.29	2.01±0.13	ND	ND	116.1±17.2	96.3±10.9
Δ67	4.27±0.26	1.93±0.16	2.21±0.12	ND	ND	5.1±0.4	16.5±0.4
Δ121	5.16±0.28	2.49±0.19	2.07±0.11	ND	ND	10.8±0.8	1.7±0.1
Δ145	4.86±0.42	2.35±0.27	2.07±0.16	ND	ND	0.8±0.1	24.0±0.4
Δ52/ Δ67	5.43±0.71	2.23±0.40	2.43±0.30	ND	ND	50.2±5.7	23.1±1.2
Δ52/ Δ121	4.09±0.57	2.32±0.44	1.76±0.23	ND	ND	51.2±2.8	0.37±0.01
Δ52/ Δ145	3.25±0.45	1.95±0.35	1.67±0.19	ND	ND	77.7±11.7	31.9±2.5
Δ67/ Δ121	ND	ND	ND	ND	ND	5.6±0.7	0.38±0.02
Δ67/ Δ145	ND	ND	ND	ND	ND	4.8±0.1	41.1±0.4
Δ121/ Δ145	3.21±0.78	1.89±0.59	1.70±0.34	ND	ND	7.3±0.4	0.22±0.00

^a ΔG_u° , C_m , m , v° , and β_s° values were measured at pH 7.0 and 15°C. K_m and k_{cat} values were measured at pH 7.0 and 25°C. Taken from Gekko et al. [31,32,77], Ohmae et al. [33–35,64], and Horiuchi et al. [72].

ND, not determined. Data are mean±SD values.

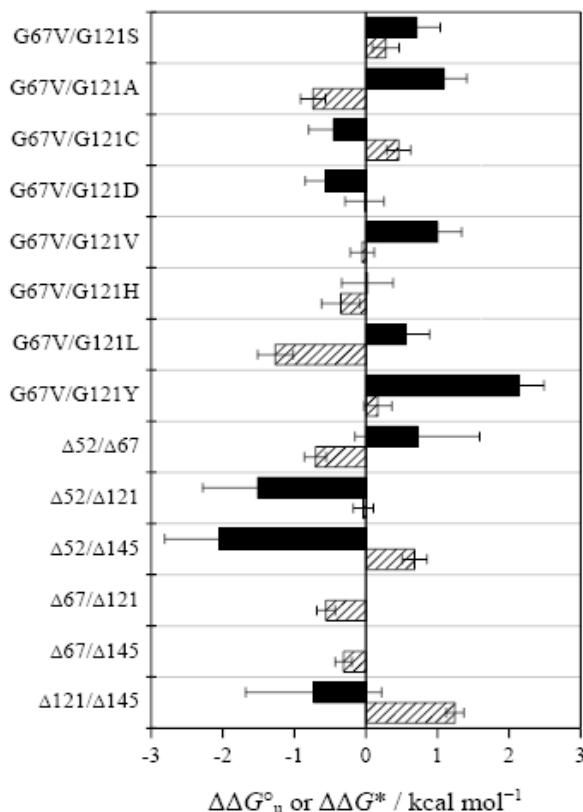


Figure 3: Nonadditive effects of double mutations in flexible loops on stability, $\Delta\Delta G_u^\circ$ (filled bars), and enzyme function, $\Delta\Delta G^*$ (hatched bars). These values were calculated using the following equations with data in **Table 1**:

$$\Delta\Delta G_u^\circ = (\Delta G_{u,XY}^\circ - \Delta G_{u,X}^\circ) - (\Delta G_{u,Y}^\circ - \Delta G_{u,\text{wild-type}}^\circ)$$

$$\Delta\Delta G^* = RT \ln \left[\frac{\{(k_{cat}/K_m)_X \cdot (k_{cat}/K_m)_Y\}}{\{(k_{cat}/K_m)_{XY} \cdot (k_{cat}/K_m)_{\text{wild-type}}\}} \right]$$

where the subscripts X and Y attached to ΔG_u° and k_{cat}/K_m denote the single mutants and X/Y denotes the corresponding double mutant [35].

The thermal stability of ecDHFR is also influenced by loop mutations [31,32,69]. The thermal transition temperatures of eight mutants at residue 121 were within the range of 43.8–46.9°C, and so were lower than that of the wild type (49.3°C). The calorimetric enthalpy of denaturation also decreased, and so the destabilization of these mutants was attributed to an enthalpy effect rather than an entropy effect. In most mutants, the ratios of the van't Hoff enthalpy to the calorimetric enthalpy were smaller than unity (actually around 0.5), suggesting that the thermal denaturation cannot be explained by a two-state unfolding mechanism and that at least one intermediate exists during the process of thermal denaturation [32,69,70]. Such an intermediate was also observed in the acid denaturation of wild-type ecDHFR around a pH of 4 at 15°C [70]. Judging from the similarity of the circular dichroism (CD) spectra, the intermediates found in both types of denaturation may be a molten globule such as that involved in the folding kinetics [71].

2.1.2. Loop-residue deletion

Since the deletion of a loop residue shortens the loop and reduces flexibility, a deletion mutation is expected to have greater structural and dynamical impacts on the corresponding part than does a substitutive mutation, and hence will amplify the effects caused by distal mu-

tations and so make the mutual couplings among the distant residues more apparent.

The values of ΔG_u° , m , and C_m for deletion mutants at residues 52, 67, 121, and 145, which are denoted as $\Delta 52$, $\Delta 67$, $\Delta 121$, and $\Delta 145$, respectively, are listed in **Table 1** [72]. These deletion mutants showed marked reductions in stability but only marginal changes in m values. The small changes in m values suggest that the solvent-accessible surface areas in the mutant proteins do not differ markedly from that of the wild type. $\Delta 67$, $\Delta 121$, and $\Delta 145$ showed more significant reductions in structural stability than did those for the corresponding substitution mutants, although the changes in m values for these mutants were not significant as the changes observed for the corresponding substitution mutants (**Table 1**). Therefore, the destabilization induced by deleting these loop residues may be attributed to changes in flexibility of the loops as suggested by the findings of substitutive mutation studies [32–34]. In contrast to the other three deletion mutants, $\Delta 52$ retained stability comparable to that of wild type, and its change in m value was also small, although deleting residue 52 may alter the flexibility of the αC – βC loop by pinching this loop. This finding suggests that deleting this residue caused little structural change, as expected from the small changes in the CD spectrum. The marginal stability change in $\Delta 52$ may be due to Arg52 being an ionic residue that is highly exposed to the solvent, although the other three residues tested are all hydrophobic and exhibit somewhat varied structures. In spite of the small change in the stability of $\Delta 52$, this deletion caused significant functional changes [72].

The possibility of couplings between the distal loops was also explored using double-deletion mutants (**Figure 3**). Considering experimental errors, $\Delta 52/\Delta 67$ and $\Delta 121/\Delta 145$ showed additive decreases in stability, indicating the absence of any apparent coupling between the αC – βC and βC – βD loops or between the βF – βG and βG – βH loops regarding structural stability. On the other hand, $\Delta 52/\Delta 121$ and $\Delta 52/\Delta 145$ showed nonadditive or synergistic destabilization: the motional and structural change in the αC – βC loop resulting from deleting residue 52 enhances the destabilization by $\Delta 121$ or $\Delta 145$, probably through modulating the motional correlation between the corresponding loops. This implicates the existence of interplay between the αC – βC loop and the βF – βG or βG – βH loop that modulates the structural stability.

2.2. Effects of loop mutations on flexibility

The protein dynamics of ecDHFR and its mutants have been investigated using various techniques aimed at determining their magnitude and timescales: the B-factor of X-ray crystallography [8,47,73], order parameter of NMR [48,63,74,75], fluorescence relaxation time [16], compressibility [76–79], and MD simulations [18,51,54,62]. Among these techniques, compressibility gives unique information on the volume fluctuation of the protein structure although it does not provide atomic resolution or timescale information, in contrast to X-ray crystallography, NMR, and fluorescence spectroscopy. Only small changes have often been

detected in the X-ray crystal structures of many proteins, even in cases where ligand binding and mutation clearly induce large differences in function and stability. However, the compressibility sensitively reflects modification of the internal atomic packing due to such local structure changes. Thus, the compressibility changes due to ligand binding [78] and mutation [76, 77] give useful information for understanding the structure–flexibility–function relationships of a protein, although such data are scarce due to the associated experimental difficulties.

2.2.1. Compressibility

There are many packing defects (cavities) in the interior of a protein molecule that allow internal motions or flexibility to thermal or mechanical forces. Such cavities are easily compressed by pressure, and hence compressibility is an important measure of protein dynamics and volume fluctuation. According to statistical thermodynamics, the volume fluctuation $\langle \Delta V_M^2 \rangle$ of a molecule with volume V_M is related to its isothermal compressibility coefficient $\beta_{T,M}$ [80] according to

$$\langle \Delta V_M^2 \rangle = k_B T V_M \beta_{T,M} \quad (2)$$

where k_B is the Boltzmann constant and T is the absolute temperature. The volume fluctuation of a protein molecule in solution may be estimated by assuming an analogous equation in which V_M and $\beta_{T,M}$ are replaced by the corresponding partial quantities [79,81]. The coefficient of partial specific compressibility of a protein molecule in solution, β^o , is defined as the pressure derivative of the partial specific volume (v^o), which consists of three contributions: the constitutive atomic volume (v_c), the cavity volume (v_{cav}), and the volume change due to solvation or hydration (Δv_{sol}). Since the constitutive atom is assumed to be incompressible, the experimentally observed β^o value of a protein can be mainly attributed to the pressure effects on two volumetric terms, v_{cav} and Δv_{sol} [79,81]:

$$v^o = v_c + v_{cav} + \Delta v_{sol} \quad (3)$$

$$\beta^o = -(1/v^o)(\partial v^o / \partial P) = -(1/v^o)[(\partial v_{cav} / \partial P) + (\partial \Delta v_{sol} / \partial P)] \quad (4)$$

The first and second terms on the right-hand side of Eq. 4 contribute positively and negatively, respectively, to β^o , and so β^o is sensitively affected by the protein structure. Although direct measurement of isothermal compressibility is technically difficult for proteins, adiabatic one β_s^o can be determined using precise sound velocity and density measurements. The β_s^o values have been measured for more than 50 proteins in water or dilute buffer solutions by many groups, with the largest set of β_s^o data of proteins including mutants having been reported by Gekko and coworkers [77,79,81].

The v^o and β_s^o values of various substitution mutants at residues 67, 121, and 145 are listed in **Table 1** [77]. A particularly interesting finding was that these loop mutations induce

large changes in ν^o (0.710 to 0.733 cm³ g⁻¹) and β_s^o (-1.8 to 5.5 Mbar⁻¹) from the corresponding values of wild-type enzyme ($\nu^o = 0.723$ cm³ g⁻¹, $\beta_s^o = 1.7$ Mbar⁻¹). Since the amount of hydration and constitutive atomic volume should be hardly affected by substituting 1 of 159 amino acid residues, these changes in β_s^o and ν^o could be dominantly attributed to modifications of internal cavities.

The positive correlation ($r = 0.70$) between β_s^o and ν^o supports that cavities contribute significantly to the changes in flexibility induced by mutations. The β_s^o value tends to decrease with the increased volume of an introduced amino acid ($r = -0.66$), and hence the structural flexibility seems to be reduced by introducing a bulky side chain. This implies that the loop mutations affect not only the local atomic packing around the mutation sites, but also the internal cavities throughout the protein molecule *via* long-range interaction effects. We observed significant changes in the B-factors of the main-chain atoms and the cavities at positions far from mutation residues 67 and 121 (unpublished data). Moreover, computer simulations predicted that Gly67 and Gly121 cannot be replaced by any other amino acid residues without accompanying movements of the backbone polypeptide chain. Thus, a single amino acid substitution in these loops dramatically influences the flexibility of ecDHFR by modifying the atomic packing, which leads to modification of the enzyme function. A high-pressure NMR study of folate-bound ecDHFR revealed that these loop regions are greatly affected by pressure as well as hinge motion of the Met20 loop: the ¹⁵N/¹H-HSQC (heteronuclear single quantum coherence) spectra at 200 MPa showed a significant decrease in cross-peak intensity for residues 5, 12, 15, 23, 37, 52, 54, 67, 79, and 124, and a splitting of signals for residues 12, 13, 22, 51, and 95 [75]. These data support that loop regions play important roles in protein dynamics and function *via* atomic packing. Since no definite correlation was found between β_s^o and ΔG_u^o , the rigid mutant is not necessarily stable against urea.

2.2.2. Hydrogen/deuterium exchange

The exchange of amide hydrogen to deuterium (H/D exchange) of the polypeptide backbone has been widely used as a measure of protein dynamics because the rate and number of exchangeable amide hydrogen atoms can be determined concomitantly. The H/D exchange kinetics of a protein has been explained by the local-unfolding model or EX₂ mechanism in which the rate of exchange (k_{ex}) is determined by the transient opening of the folded structure [82,83]. Although H/D exchange has often been monitored by infrared spectroscopy and NMR [84,85], recent developments in mass spectrometry (MS) have provided a new method for analyzing the H/D exchange of proteins [82,86,87].

The H/D exchange kinetics of ecDHFR have been studied using matrix-assisted laser desorption/ionization time-of-flight (TOF) MS analysis combined with pepsin digestion to elucidate the backbone-fluctuation map [88]. The 18 digestion fragments covering almost

the entire amino acid sequence exhibited significant variations in k_{ex} (0.47–0.71 min⁻¹), in the fraction of deuterium incorporation at the initial stage ($D_o = 0.20$ –0.60), in the fraction of deuterium incorporation at infinite time ($D_\infty = 0.75$ –0.97), and in the number of hydrogen atoms protected from exchange ($N_p = 0.4$ –4.7) relative to the corresponding values for the entire ecDHFR molecule ($k_{ex} = 0.51$ min⁻¹, $D_o = 0.41$, $D_\infty = 0.85$, and $N_p = 20.7$). The H/D exchange process was very rapid in the fragment comprising residues 5–28 (Met20 loop), rapid in disordered and hydrophobic fragments, but slow in β -strand-rich fragments. These results indicate that each fragment makes a different contribution to the fluctuations of the ecDHFR molecule.

The H/D exchange kinetics parameters of the substitution mutants at residues 67 and 121 were also determined by electrospray ionization TOF MS [89]. These mutations induced significant changes in k_{ex} (0.10–0.27 min⁻¹), in the number of fast-exchangeable hydrogen atoms ($\Delta M_o = 164$ –222 Da), and in the number of hydrogen atoms protected from exchange ($\Delta M_\infty = 15$ –56 Da) relative to the corresponding values for the wild-type enzyme ($k_{ex} = 0.18$ min⁻¹, $\Delta M_o = 164$ Da, and $\Delta M_\infty = 50.5$ Da). These kinetics parameters were strongly correlated with the volume of introduced amino acids and weakly correlated with β_s^o and ΔG_u^o . Thus, H/D exchange data as obtained using MS also support that the loop mutations significantly affect the structural fluctuations of the entire molecule.

2.3. Effects of loop mutations on function

As shown in **Figure 2**, ecDHFR catalyzes the reduction of DHF to THF with the aid of coenzyme NADPH *via* five intermediates: DHFR·NADPH, DHFR·NADPH·DHF, DHFR·NADP⁺·THF, DHFR·THF, and DHFR·NADPH·THF. The effects of mutation on these steps have been examined *via* steady-state and pre-steady state kinetics measurements [16, 49]. The rate constants for ligand binding or releasing, most of which have been measured by Benkovic's group, are important to better understand the catalytic mechanism of ecDHFR and its mutants. Intrinsic kinetic isotope effects on hydride transfer have revealed the correlation of network motions to catalytic reaction [45,60,61]. Although the steady-state kinetics based on the overall rate-determining step cannot present such detailed information on the modified steps in catalytic reaction, they are valuable for comparatively diagnosing the effects of mutation on the catalytic function.

2.3.1. Loop-residue substitution

The steady-state kinetics parameters K_m and k_{cat} for the substitution mutants at residues 42, 67, 121, and 145 are listed in **Table 1** [31–34,64]. It is evident that these parameters are dependent on the mutants, resulting in a definite modification of the enzyme activity (k_{cat}/K_m). It is unlikely that these distal residues participate directly in the enzyme reaction because the α -carbons of Gly67, Gly121, and Ala145 are 29.3, 19.0, and 14.4 Å, respectively, from the

catalytic residue Asp27, and their shortest distances from the NADPH molecule are 8.5, 10.6, and 29.2 Å. The Gly121 mutant was the one that showed significantly lower k_{cat}/K_m values than the wild-type enzyme (at most a 42-fold decrease for G121L), primarily due to a reduced turnover rate (k_{cat}) and little change in the substrate-binding ability (K_m) [31,32]. Although to our knowledge, this was the first evidence for Gly121 participating in the function of ecDHFR, it was difficult to identify the affected steps within the catalytic cycle from knowledge of the steady-state kinetics only. Cameron and Benkovic [50] used a stopped-flow analysis to reveal that G121V results in a 40-fold decrease in the NADPH-binding affinity, a 200-fold decrease in the hydride transfer rate, and a 7-fold decrease in the rate of product release. Furthermore, this mutation introduced a new step into the catalytic cycle that reflects a slow conformational change prior to hydride transfer and probably involves exchange of the nicotinamide ring of NADPH into the active site to form the Michaelis complex [50]. Many subsequent experimental and theoretical studies have demonstrated the important roles of this residue in dynamics and function of ecDHFR [17,59,60,69,90–93].

In contrast to Gly121 mutants, mutations at residues 67 and 145 caused marginal disturbance to enzymatic catalysis, although they significantly changed the structural stability (**Table 1**) [33,34]. The flexibility of Gly67 has been found to be functionally irrelevant [17], but this residue showed motional correlation with the Met20 loop in the MD simulations of the Michaelis complex (DHFR·NADPH·DHF), as found for Gly121 [54,56,69]. According to the explanation for the effects of Gly121 on the enzyme reaction, Gly67 is anticipated to disturb catalysis somewhat. The rate of hydride transfer from NADPH to DHF was influenced by mutations at residue 67, although K_m and k_{cat} were influenced only slightly; hydride transfer was fully rate-determining for G67C and G67D while only partially rate-determining for G67S, G67L, and G67T [33]. On the other hand, Ala145 did not show any apparent motional correlation with the residues in the Met20 loop, but it was correlated with the residues around Met42 that are strongly correlated with the Met20 loop [18]. Therefore, Ala145 mutants would be expected to indirectly disturb catalysis *via* the motional coupling with Met42.

Both the K_m and k_{cat} values of Met42 mutants increased with the side-chain hydrophobicity, with the M42W mutant showing exceptionally large increases in K_m (35-fold) and k_{cat} (4.3-fold) relative to the wild-type enzyme [64]. Such significant effects of Met42 mutants might be consistent with MD simulations of the Michaelis complex showing correlated motion between the regions containing Met42 and Gly121 [18, 60]. Thus, Met42 is an important distal residue for the function of this enzyme, and is correlated with the dynamics of the Met20 and other loops.

Double-substitution mutants at residues 67 and 121 exhibited only small changes in K_m but large changes in k_{cat} (**Table 1**). These changes could be mainly accounted for by Gly121-inducing effects. The transition-state stabilization energy defined as $-RT\ln(k_{cat}/K_m)$ of G67V/

G121A, G67V/G121C, and G67V/G121L was obviously not equal to the sum of the values for the corresponding single mutants (**Figure 3**) [35]. Thus, the additivity rule does not hold for these double mutants, and there exist long-range interactions (motional coupling) between both residues, as found for the stability of double mutants. Double mutants at residues 42 and 121 also showed nonadditive or synergistic decreases in hydride transfer rates with small or negligible changes in other enzymatic parameters [17], suggesting that the two distal residues are coupled in dynamic processes so as to organize the Michaelis complex into the active form.

2.3.2. Loop-residue deletion

The steady-state kinetics parameters K_m and k_{cat} for $\Delta 52$, $\Delta 67$, $\Delta 121$, and $\Delta 145$ mutants are listed in **Table 1** [72]. It is evident that deleting these residues induced changes in K_m and k_{cat} , resulting in a definite modification of the enzyme activity (k_{cat}/K_m) as was also found for substitutive mutations. Marked reductions in both K_m and k_{cat} of $\Delta 121$ are consistent with Miller and Benkovic [90] finding that in contrast to the substitutive mutation of Gly121, the deletion of Gly121 dramatically decreased the rate of hydride transfer (by 550-fold) and the cofactor-binding strengths for NADPH and NADP⁺ (by 20-fold and 7-fold, respectively). The marked reduction in the hydride transfer rate can be attributed to the deformed Michaelis complex of $\Delta 121$, which may have poorly coordinated ligands for the enzymatic reaction. These results for $\Delta 121$ have demonstrated the important dynamic role of the βF – βG loop in ecDHFR catalysis through its greater structural perturbation compared to the substitutive mutation of Gly121 [17,50].

$\Delta 67$ showed greatly reduced activity compared to the corresponding substitution mutants, suggesting that deletion of Gly67 has a greater impact on the βC – βD loop than does amino acid replacement (**Table 1**). Since $\Delta 67$ showed an apparent stability reduction without any gross structural change, as judged from its m value and CD spectrum, the reduced activity could hardly be attributed to structural deformation. Similar to the effects of substitutive mutation at residue 121, the effect of deleting residue 67 may be due to motional coupling between the βC – βD and Met20 loops, which was predicted by MD simulations [18].

$\Delta 145$ had unexpectedly greater activity than the wild type mainly due to the decreased K_m , since k_{cat} remained at almost the same level as in the wild type. $\Delta 145$ also showed reduced structural stability, but with no apparent overall structural change revealed by the CD spectrum. The deletion of Ala145 may induce motional or conformational changes of the βG – βH loop, or both types of changes, that propagate to the DHF-binding site and enhance its binding. The motional correlation map simulated by MD for the Michaelis complex revealed only a slight correlation between the βG – βH loop and the αB helix (residues 24–35), which is a binding scaffold for DHF [18]. This result suggests that the increased affinity of DHF could be

attributable to structural rearrangement around the DHF-binding site, although a change in the dynamics at the residue cannot be ruled out since Ala145 exhibits a motional correlation with the residues around Met42 that are strongly correlated with the Met20 loop. This highlights the spatial proximity of Ala145 to the DHF-binding site.

$\Delta 52$ has another remarkable feature of a 100-fold reduction in ligand-binding strength and a 4-fold increase in k_{cat} . Since the αC – βC loop is spatially close to DHF in the Michaelis complex (**Figure 1**), the large changes in K_m may be explained by the depletion of ionic interactions between DHF and Arg52, while the changes in k_{cat} may be explained by dynamic and conformational changes induced by deleting this residue. However, the marked changes in k_{cat} of $\Delta 52$ cannot be readily explained using the available dynamic data because the αC – βC loop does not appear to be correlated with the other regions of the protein in the MD-derived motional correlation map. Although the αC – βC loop has not been focused, it could be another hotspot that modulates enzymatic activity. Deletion of two residues 45 and 46 in the loop region (residues 40–46) in human DHFR has also been shown to affect stability and function *via* the modification of structural flexibility [94].

In all of the double-deletion mutants tested ($\Delta 52/\Delta 67$, $\Delta 52/\Delta 121$, $\Delta 52/\Delta 145$, $\Delta 67/\Delta 121$, $\Delta 67/\Delta 145$, and $\Delta 121/\Delta 145$), the effect of a second mutation was found to be nonadditive except for $\Delta 52/\Delta 121$, with prominent nonadditivity for $\Delta 121/\Delta 145$ and marginal effects for $\Delta 67/\Delta 145$ (**Figure 3**). The loops containing Gly121 and Ala145 are both engaged in hydride transfer and product release in the wild type. The significant nonadditive effect found for $\Delta 121/\Delta 145$ could therefore be explained by the Met20 loop changing the hydrogen-bonding partner from βF – βG to βG – βH loops harboring the respective residues 121 and 145, according to the enzyme reaction [8]. It should be noted that $\Delta 121/\Delta 145$ showed an additive effect on the structural stability but a nonadditive effect on the function. This is possible because the stability is related to the free energies of both the native and denatured states, whereas the enzyme function is only relevant to the native state. $\Delta 67/\Delta 121$ also showed more significant effects than the double-substitution mutants between residues 67 and 121. Although the magnitudes of the effects differed, the statistically observed significant nonadditivity for all of the combinations of deletion residues clearly indicates that the loops tested have functional interdependence.

2.3.3. Relationship between flexibility and function

The relationships between structural dynamics and catalytic function of ecDHFR have been discussed in many experimental and theoretical investigations as summarized in recent reviews [42–46]. These studies have revealed or predicted the network of coupled motions including various distal residues correlated to catalytic function, demonstrating the significance of the distal residues. An interesting problem is whether the overall structural flexibility of ecDHFR takes part in the catalytic function.

A comparison between β_s^o and the steady-state kinetics parameters gives useful information on the flexibility–function relationship, although β_s^o gives no motional features of the fluctuating enzyme. **Figure 4** shows plots of the β_s^o values of kinetics intermediates in the reaction pathway, in which the β_s^o value of the transient DHFR·NADPH·DHF complex—which is unobtainable as a stable complex—was assumed to be the same as that of the ternary complex DHFR·NADPH·MTX based on the structural similarity of the two ternary complexes [78]. β_s^o changes when the coenzyme and substrate are bound or released, while the transient state DHFR·NADPH·DHF is the most flexible and the DHFR·NADP⁺·THF is the most rigid of the intermediates. Similar changes in the flexibility during the reaction cycle were also assumed from the H/D exchange of kinetics intermediates [95]. These findings indicate that the structural flexibility changes significantly during the catalytic cycle. This is consistent with a movie constructed by Sawaya and Kraut [8] showing that the loops move actively and cooperatively to accommodate both the coenzyme and substrate. The ligand binding caused slight changes (at most 6%) in the solvent-accessible surface area but large changes in the total cavity volume (up to 40%) of ecDHFR. The number, size, and distribution of cavities were correlated with the changes in β_s^o (**Figure 5**). These results suggest that the changes in the flexibilities of the intermediates are dominantly attributable to changes in the cavities [78,79].

Neutron scattering experiment [96] and normal mode analysis [97] showed a softening of vibrational dynamics of ecDHFR on binding MTX to DHFR·NADPH. This result indicates an enhancement of the degrees of freedom responsible for volumetric changes of the protein, consistent with increased β_s^o of the system. It is noticeable that the most significant softening of vibrational dynamics is found in the loops of the protein containing the residues Gly67, Gly121, and Ala145, which have the large effects on stability and function on site-directed mutagenesis [97].

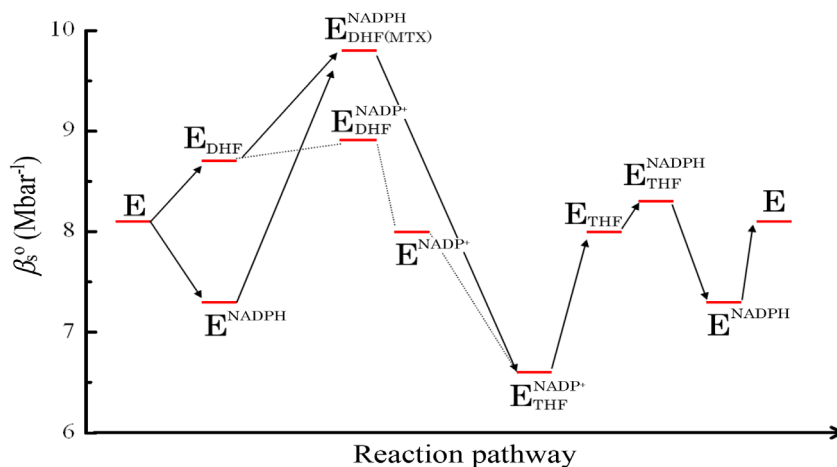


Figure 4: Changes in β_s^o of the kinetics intermediates of ecDHFR in the reaction pathway. MTX refers to methotrexate and other abbreviated letters are the same as in **Figure 2**. The β_s^o value of the transient state DHFR·NADPH·DHF was assumed to be the same as that of the ternary complex DHFR·NADPH·MTX. (Reproduced from Kamiyama and Gekko [78]).

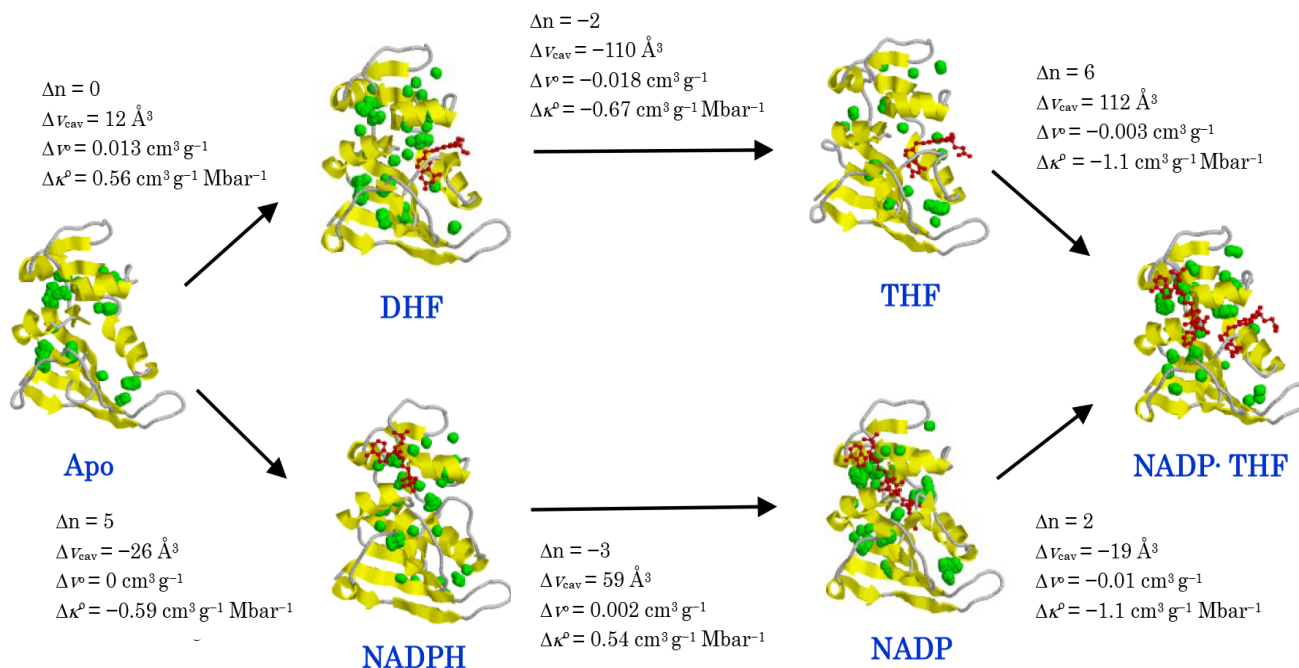


Figure 5: Changes in the number of cavities (Δn), cavity volume (ΔV_{cav}), partial specific volume (Δv°), and adiabatic compressibility [$\Delta \kappa^\circ = \Delta(v^\circ \beta_s^\circ)$] of ecDHFR due to ligand binding. Cavities are shown by green balls. (Reproduced from Kamiyama and Gekko [78].)

Figure 6 shows plots of the K_m and k_{cat}/K_m values against β_s° for loop substitution mutants. Although the correlations are not significant, β_s° appears to be negatively correlated with K_m ($r = -0.632$) and positively correlated with k_{cat}/K_m ($r = 0.552$), mainly due to the positive correlation between k_{cat} and β_s° ($r = 0.41$), with the exception of three mutants (G67T, G67L, and G121V) associated with large experimental errors in β_s° ($>1 \text{ Mbar}^{-1}$). This correlation suggests that the structural flexibility contributes favorably to the enzyme function by enhancing substrate binding and product release, with the latter mechanism dominating. This is supported by a very large β_s° value observed for a hyperactive ecDHFR mutant along with k_{cat} being sevenfold higher than for the wild type, in which all five methionine and two cysteine residues were replaced by other amino acid residues using a molecular evolutionary technique [98]. A similar positive correlation between β_s° and enzyme function was found for mutants of *E. coli* aspartate aminotransferase at Val39, which is located at the gate of a substrate-binding site [76]. Mutations at residues distant from DNA and cyclic adenosine monophosphate (cAMP)-binding sites of *E. coli* cAMP-receptor protein also induced large changes in β_s° that were very clearly correlated with the free energy of DNA binding ($r = 0.935$) and the difference in free energy of binding of two cAMP molecules ($r = -0.980$) [99]. This demonstrates that the structural flexibility plays an essential role in modulating the DNA binding and the allosteric behavior of the protein.

Together with the mutation effects on β_s° of the proteins examined so far, a one-unit increase in β_s° is assumed to enhance the function of the protein by about tenfold. This suggests that the overall fluctuation of protein molecule, being constructed by a complicated mo-

tional hierarchy, is significant in protein function. Although β_s^o does not reveal microscopic features of the structural fluctuation, it should be emphasized that the local structural changes due to loop mutations are dramatically magnified in the overall protein dynamics through the modified cavities so as to affect the enzyme function. Such viewpoint when introduced into experimental and theoretical studies might lead to a deeper understanding of the cooperative interactions between distal residues and the motional network around the active site.

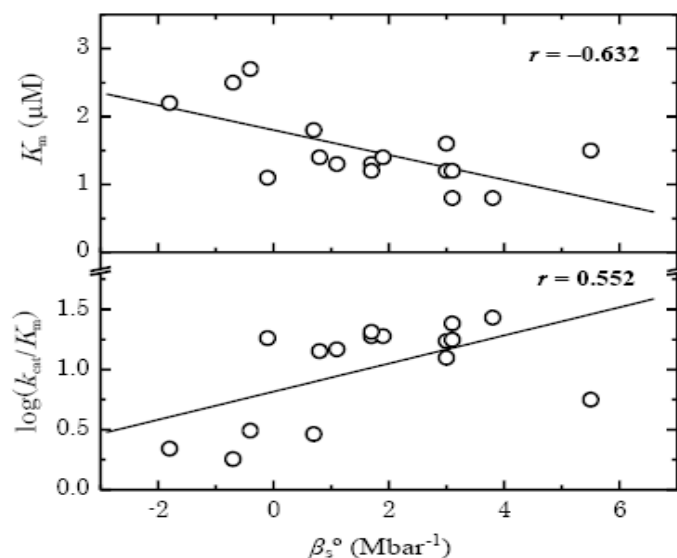


Figure 6: Plots of K_m and $\log(k_{cat}/K_m)$ against β_s^o for site-directed substitution mutants at flexible loops of ecDHFR. Solid lines are least-squares linear regressions. (Reproduced from Gekko et al. [77].)

3. DHFRs from Deep-Sea Bacteria

The deep sea is an extreme environment characterized by high hydrostatic pressure up to 110 MPa (a depth of 11,000 m). There live many microorganisms or bacteria depending on the depth: piezophilic, piezosensitive, and piezotolerant species. The pressure adaptation of these deep-sea bacteria has been mainly studied in terms of gene regulation [100–102], but there are limited information at the protein level because the characterization of deep-sea proteins is experimentally difficult. DHFR is a good target enzyme for studying the pressure-adaptation mechanisms of deep-sea proteins because it is an essential enzyme in all the living cell.

As found for ecDHFR, the β_s^o value changes with the kinetics pathway and the enzymatic activity of mutants [77,78,98]. A high-pressure NMR analysis revealed the existence of a pressure-dependent open conformer that would be crucial for NADPH binding [75]. These results suggest that DHFRs from deep-sea bacteria exhibit unique pressure susceptibility and structural dynamics different from those of organisms living under atmospheric pressure. Although the enzymatic activity of ecDHFR decreased with increasing pressure [103], DHFR from *Shewanella violacea* strain DSS12 (svDHFR) isolated from the Ryukyu Trench at a depth of 5,110 m [104,105] was found to exhibit optimal activity at approximately 100 MPa [106]. Therefore, comparative studies of DHFRs from deep-sea and atmospheric-pressure bacteria

should yield useful information for understanding the flexibility–function relationship and the molecular or evolutionary adaptation mechanism of this enzyme to high-pressure environments.

We cloned 17 DHFRs from 11 piezophilic, 5 piezosensitive, and 1 piezotolerant bacterial species isolated from various environments, as listed in **Table 2** [37–40]. The pressure effects on the stabilities and enzymatic activities of 10 of these DHFRs are considered in terms of the internal cavities and surface hydration compared with those of ecDHFR in order to elucidate the species-dependent pressure susceptibility and structural flexibility.

Table 2: DHFR names and original bacterial species described in this study^a.

DHFR name	Bacterial species	Isolation source or depth	Piezophilicity
sb43992DHFR	<i>S. benthica</i> ATCC43992	4,575 m	Piezophilic
sb21DHFR	<i>S. benthica</i> DB21MT-2	10,898 m	Piezophilic
sb6705DHFR	<i>S. benthica</i> DB6705	6,356 m	Piezophilic
sfDHFR	<i>S. frigidimarina</i> ACAM591	Antarctic sea ice	Piezosensitive
sgDHFR	<i>S. gelidimarina</i> ACAM456	Antarctic sea ice	Piezotolerant
soDHFR	<i>S. oneidensis</i> MR-1	Oneida Lake	Piezosensitive
spDHFR	<i>S. putrefaciens</i> IAM12079	rancid butter	Piezosensitive
svDHFR	<i>S. violacea</i> DSS12	5,110 m	Piezophilic
maDHFR	<i>M. abyssi</i> 2693	2,815 m	Piezophilic
mjDHFR	<i>M. japonica</i> DSK1	6,356 m	Piezophilic
mmDHFR	<i>M. marina</i>	seawater	Piezosensitive
mpDHFR	<i>M. profunda</i> 2674	2,815 m	Piezophilic
myDHFR	<i>M. yayanosii</i> DB21MT-5	10,898 m	Piezophilic
ppDHFR	<i>P. phosphoreum</i>	seawater	Piezosensitive
ppr4DHFR	<i>P. profundum</i> DSJ4	5,110 m	Piezophilic
ppr9DHFR	<i>P. profundum</i> SS9	2,551 m	Piezophilic
pkDHFR	<i>Psychromonas kaikoae</i> JT7304	7,434 m	Piezophilic
ecDHFR	<i>E. coli</i>		Piezosensitive

^aTaken from Ohmae et al. [40].

3.1. Primary and tertiary structures of deep-sea DHFRs

Figure 7 shows the primary structures of deep-sea DHFRs and their normal homologs from congeneric species living in an atmospheric-pressure environment (the nomenclature of each DHFR is listed in **Table 2**). These DHFRs consist of approximately 160 amino acid residues independent of species. The amino acid sequence is considerably conserved at the N-terminal region but highly variable at the C-terminal region. The active-site residue, which is Asp27 in ecDHFR, is completely conserved as Asp28 or Glu28 in all DHFRs. These results suggest that all of these DHFRs adopt a similar folded structure to maintain the catalytic func-

tion.

We determined the crystal structure of a deep-sea DHFR from *M. profunda* (mpDHFR, PDB: 2zza) [39]. The backbone structures of ecDHFR and mpDHFR almost overlap, although their sequence similarity is only 55% (**Figure 7**). Conservation of the backbone structure was also observed in other deep-sea enzymes such as 3-isopropylmalate dehydrogenase (IPMDH) from *S. benthica* strain DB21MT-2 [107], aspartate carbamoyltransferase from *M. profunda* [108], α -glucosidase from *Geobacillus* sp. strain HTA-462 [109], Cu/Zn superoxide dismutase from the deep-sea yeast *Cryptococcus liquefaciens* strain N6 [110], and superoxide dismutase from the deep-sea worm *Alvinella pompejana* [111]. Homology modeling also suggests that deep-sea enzymes have the same folded structures as their normal homologs [112–115]. Human and mouse DHFRs have a similar backbone structure to ecDHFR [116,117] although the sequence similarity is very low (29%), which is comparable to that of 32% for mjDHFR (from *M. japonica* strain DSK1). Considering these results, other deep-sea DHFRs with unknown X-ray structures are expected to have essentially the similar tertiary structures as that of ecDHFR, although their sequence similarity is not particularly high (48–56% in most cases).

	10	20	↓30	40	50	60	70	80	90
sb43992DHFR	-MKIAMIV A MANNRV I GKDNK MP WHLPE LKH F K A M T L G K P I V M G R K T Y E S I G R A L P G R L N I V I S R Q E G L S I A G V T C V T S F E S A V A A A G E C								
sb6705DHFR	-MKIAMIA A MANNRV I GKDNK MP WHLPE LKH F K A M T L G K P I V M G R K T Y E S I G R A L P G R L N I V I S R Q E G L S I A G V T C V T S F E S A V A A A G E C								
sb21DHFR	-MKIAMIA A MANNRV I GK N Q M WHLPE LKH F K A M T L G K P I V M G R K T Y E S I G R A L P G R L N I V I S R Q Q L T I P G V T C V T S F E S A V A A A G E C								
svDHFR	-MKIAMIA A MANNRV I GKDN Q M P WHLPE LKH F K A M T L G K P I V M G R K T Y D S I G R A L P G R L N I V I S R Q E G L S I P G V T C V T S F E M A V E A A G E C								
sgDHFR	ILKIAMIA A MANNRV I GKDNK MP WHLPE LKH F K A V T L G K P I V M G R K T Y E S I G R P L P G R H N I V I S R Q A D L A I D G V T T V T C F E D A K L A A G D C								
spDHFR	-MRIAMIA A MANNRV I GKDNK MP WHLPE LKH F K A M T L G K P V M G R K T F E S I G R P L P G R H N I V I S R Q A D L V I E G V T S V T S F D A A K Q A A G E C								
soDHFR	-MRIAMIA A MANNRV I GKDNK MP WHLPE LKH F K A M T L G K P V M G R K T F E S I G R P L P G R H N I V I S R Q A D L Q I E G V T C V T S F E A A K R V A G D C								
sDHFR	-MRIAMIA A MANNRV I GKDNK MP WHLPE LKH F K A M T L S K P V M G R K T Y E S I G R P L P G R H N I V I S R N S Q L S I E G V T C V K S F D E A I T V A G D C								
mmDHFR	----MIA A L A NNRV I G L D N K M WHL P A E L Q L F K R A T L G K P I V M G R N T F E S I G R P L P G R L N I V L S R Q R D Y V A E G V T V V A T L E D A I V A A G D V								
mjDHFR	-MKLSL M A A K S K N G V I G N G P D I P W Q A K G E Q L L F K A M T Y N Q W L L V G R K T F E S M G T L P N R K Y A V I S R S D F V S E D E N V M V F S I E S A L R Q L A D I								
myDHFR	----MIA A L A NNRV I G L D N K M WHL P A E L Q L F K R A T L G K P I V M G R N T F E S I G R P L P G R L N I V L S R Q T D Y Q P E G V T V V A T L E D A V V A A G D V								
mpDHFR	-MIVSMIA A L A NNRV I G L D N K M WHL P A E L Q L F K R A T L G K P I V M G R N T F E S I G R P L P G R L N I V L S R Q T D Y Q P E G V T V V A T L E D A V V A A G D V								
maDHFR	----MIA A L A NNRV I G L D N K M WHL P A E L Q L F K R A T L G K P I V M G R N T F E S I G R P L P G R L N I V L S R Q T D Y Q P E G V T V V A T L E D A V V A A G D V								
pkDHFR	----MIA A L A NNRV I G L D N K M WHL P A E L Q L F K R A T L G K P I V M G R N T F E S I G R P L P G R L N I V L S R Q T G Y Q P E G V T V V A T L E D A V I A A G D V								
ppDHFR	-MKIS M I A M A H D R I I G K D N S M P WHL P A D F A W F K R C T L G K P I V M G R K T F E S I G R P L P G R L N I V I S R N P N F T A E G I T V V S D I A A K L V A G D A								
ppr4DHFR	----MIA A M A K D R V I G K D N A M P WHL P A D F A W F K S T L G K P I V M G R K T F E S I G R P L P G R L N I V I S R N P E F S V E G V T V V A D I E A A K H A A G D I								
ppr9DHFR	----MIA A M A K D R V I G K D N A M P WHL P A D F A W F K S T L G K P I V M G R K T F E S I G R P L P G R L N I V I S R N P E F S V E G V T V V A D I E A A K H A A G D I								
ecDHFR	--MIS L I A L A V D R V I G M E N A M P W N L P A D L A W F K R N T L N K P V I M G R H T W E S I G R P L P G R K N I L S S Q P --G T D D R V T W V K S V D E A I A C G D V								

	100	110	120	130	140	150	160	Length	Similarity	
sb43992DHFR	EELV I GGG-QL Y AALLSQADK L YL T E I N L D V D G D T H F PRWDDGSWQR I SQ E T A I N D K G L E Y S F I N L V K K -----							160	49%	
sb6705DHFR	EELV I GGG-QL Y AALLSQADK L YL T E I N L D V D G D T H F PRWDDGSWQR I SQ E T A I N D K G L E Y S F I N L V K K -----							160	50%	
sb21DHFR	EELV I GGG-QL Y AALLSQADK L YL T E I N L D V D G D T H F QWDDGSWQR V SQ E T S I N D K G V E Y S F I N L V K K -----							160	51%	
svDHFR	EELV I GGG-QL Y ASLLSKADK L YL T E I N L D V A G D T F F QWDDGSW R I S Q E M L V N G A G L E Y S F I N L V K K -----							160	52%	
sgDHFR	EELV I GGG-QL Y TSL L C L SD V L Y L T E I S L D V E G D T F F H W D D GS W L E M S R D V A I S G K Q L E Y S F I K M V K K -----							161	48%	
spDHFR	EELV I MG G -QL Y RE L L P Q A D I L Y L T Q I N L D V E G D T F F E W D A R D W Q E T S L S C I N A D G L E Y R F I N L T K K -----							160	53%	
soDHFR	EELV I GGG-QL Y K Q L L P Q A D R L YL T Q I N L D V D G D T F F A W E D N E W Q K T E T Q P S I S A D G L E Y N F I N L V K K-----							160	48%	
sDHFR	EE I V I GGG-QL Y Q Q L L P Q A D V L YL T L I D V D V D G D T V F F A W D D G S W D L Q N S V T A T N D K G L Q S F N T L V K K-----							160	51%	
mmDHFR	EEL M I G G A -T I Y S Q C L A A A D R L Y L T H I E L T T A G D T W F P D Y E Q Y N W Q E I E Q E Y F V A D D N N P H D Y R F S L L E R V K-----							158	55%	
mjDHFR	T D H V I S GG G E I Y R S L I S K V D T L H I S T I E T E G D I V F P D I P D S F S L A F E Q K F E S N I N Y C Y I W Q N S -----							157	32%	
myDHFR	EEL M I G G A -T I Y N Q L A A A D R L YL T H I E L T I E G D T W F P D Y E Q Y H W Q E I E H E S Y A A D D K N P H D Y R F S L L E R V K-----							158	55%	
mpDHFR	EEL M I G G A -T I Y N Q L A A A D R L YL T H I E L T T E G D T W F P D Y E Q Y N W Q E I E H E S Y A A D D K N P H D Y R F S L L E R V K-----							162	55%	
maDHFR	EEL M I G G A -T I Y N Q L A A A D R L YL T H I E L T T E G D T W F P D Y E Q Y N W Q E I E H E S Y A A D D K N P H D Y R F S L L E R V K-----							158	55%	
pkDHFR	EEL M I G G A -T I Y Q Q L A A A D R L YL T H I E L T T A G D T W F P D Y E Q Y N W H E I V H E N Y S A D D K N P D Y H F S L L E R V K -----							158	54%	
ppDHFR	PE L M I I G G G -S I Y Q A C L P I A D S L Y L T F I D A D L E G D T Q F P D W G E H -- W H R V E S Q R Y N A D D K N A Y E M F V I L E R S-----								160	55%
ppr4DHFR	G E L M V I GG G -S I Y E A C L P S A D R L Y L T F I D L D V D G D T C F P D W G E G -- W I K S Y T E H S A D E K N A H D M Q F V I L D R N V D L T								160	55%
ppr9DHFR	G E L M V I GG G -S I Y E A C L P S A D R L Y L T F I D L D V D G D T C F P D W G E G -- W I K S Y T E H S A D E K N A H D M Q F V I L D R N V D L T								160	56%
ecDHFR	PE I M V I G G G -R V Y E Q L P K A Q K L YL T H I D A E V E G D T H F P D Y E P D D W E S V F S E F H D A A Q N S H S Y C F E I L E R R-----								159	100%

Figure 7: Amino acid sequences of DHFRs from deep-sea bacteria and their congeneric species. Deep-sea DHFRs are indicated by red boldface letters. Residue numbering is based on the sequence of DHFR from *S. benthica*. Conserved amino acid residues are indicated by shading, with fully conserved residues indicated by red boldface letters. The active-site residue is indicated by the arrow on the numbering row. The sequence length and similarity with ecDHFR are also indicated at the end of each sequence. (Reproduced from Ohmae et al. [40].)

Table 3: Thermodynamic parameters for urea denaturation (ΔG_u° , C_m , and m) and steady-state kinetics parameters (K_m and k_{cat}) of deep-sea and atmospheric-pressure DHFRs ^a.

DHFR	ΔG_u° (kJ mol ⁻¹)	C_m (M)	m (kJ mol ⁻¹ M ⁻¹)	K_m (μ M)	k_{cat} (s ⁻¹)
ecDHFR	26.9±3.7 (21.8±1.8) ^b	2.9±0.5 (2.7±0.3)	9.4±1.2 (8.2±0.7)	1.1±0.1	18.4±0.2
sb21DHFR	8.7±1.2	1.9±0.3	4.6±0.3	1.7±0.1	62.7±1.2
sb6705DHFR	7.9±0.9	1.7±0.2	4.7±0.3	2.0±0.2	79.1±1.6
sfDHFR	8.3±0.9	2.1±0.2	4.0±0.2	1.4±0.1	90.7±1.6
soDHFR	6.7±1.0	1.1±0.2	5.9±0.3	1.0±0.1	45.5±0.8
spDHFR	8.3±1.4	1.2±0.2	6.9±0.6	2.4±0.3	96.2±2.9
svDHFR	8.0±0.5	2.3±0.2	3.5±0.2	1.9±0.2	90.1±2.9
mjDHFR	ND	ND	ND	238±26	144.5±3.2
myDHFR	ND	ND	ND	1.8±0.2	83.8±2.4
ppr9DHFR	ND	ND	ND	6.2±0.8	156.0±5.6
mpDHFR	(7.9±0.6)	(1.8±0.2)	(4.3±0.2)		

^aThermodynamic and kinetics parameters were determined at 15°C and 25°C, respectively. Taken from Murakami et al. [37,38]. ^b Values in parentheses were determined at 25°C. Taken from Ohmae et al. [39].

3.2. Stability of deep-sea DHFRs

The ΔG_u° , m , and C_m values for urea denaturation of deep-sea DHFRs and their normal homologs are listed in **Table 3** [37–39]. The ΔG_u° and C_m values of mpDHFR and six *Shewanella* DHFRs were considerably smaller than those of ecDHFR, indicating that these seven DHFRs are less stable than ecDHFR against urea. The small difference in ΔG_u° among the six *Shewanella* DHFRs may be attributed to their high sequence similarity (more than 80%). The significantly reduced m value of these DHFRs indicates a reduction in the cooperativity of unfolding and that the solvent-accessible surface area does not increase markedly upon unfolding, probably because the native structure of these DHFRs is less compact than that of ecDHFR.

The structural stability against pressure was examined for ecDHFR and mpDHFR using fluorescence spectroscopy [39]. **Figure 8** shows the pressure dependence of the center of fluorescence spectral mass of the two DHFRs at pH 8.0 and various temperatures. It is evident that the transition of mpDHFR shifted to a lower pressure with less cooperativity compared with ecDHFR. The Gibbs free-energy change due to pressure denaturation at atmospheric pressure (0.1 MPa), ΔG_p° , was estimated by extrapolating the ΔG_p values at a given pressure P to 0 MPa:

$$\Delta G_p = \Delta G_p^\circ + P\Delta V^\circ \quad (5)$$

where ΔV° is the change in partial molar volume due to pressure denaturation at atmospheric pressure. The ΔG_p° values in the temperature region examined (15.2–28.8°C) were

16.5–21.5 and 2.9–3.3 kJ mol⁻¹ for ecDHFR and mpDHFR, respectively, indicating that mpDHFR is more unstable against pressure than is ecDHFR, as also found for urea denaturation [39]. The ΔV° value at 20.4°C was smaller for mpDHFR (–49 cm³ mol⁻¹) than for ecDHFR (–74 cm³ mol⁻¹). The volume change due to urea denaturation was also smaller for mpDHFR (–53 cm³ mol⁻¹) than for ecDHFR (–85 cm³ mol⁻¹) at 25°C [39]. Since a negative volume change can be attributed to decreased cavities and/or increased hydration upon denaturation (Eq. 3) and the denatured state should be fully solvated in both DHFRs, the smaller volume changes observed for mpDHFR could be attributed to its native structure being more loosely packed and largely hydrated than that of ecDHFR. This is consistent with the significant pressure and urea-concentration dependences of the fluorescence spectra of native mpDHFR: the solvent molecules are highly accessible to the tryptophan side chains in the interior of the mpDHFR molecule.

The thermal stability of mpDHFR is mysterious. In general, thermal denaturation of a protein as well as other types of denaturation accompany a decrease in the amount of secondary structures. This is the case for ecDHFR, but the molar ellipticity of mpDHFR at 222 nm became more negative with increasing temperature, suggesting an increase in secondary structures upon thermal denaturation [39]. Similar abnormal temperature dependences of CD spectra have been observed for other deep-sea DHFRs (svDHFR and ppr9DHFR; the latter is from *Photobacterium profundum* strain SS9), although these DHFRs aggregated upon thermal denaturation [40]. It is known that the ν° and β_s° values of native ecDHFR increase markedly with temperature and that its thermal expansion coefficient is two- or threefold higher than those of other proteins [118]. It is therefore possible that deep-sea DHFRs are more flexible at atmospheric pressure. It is unknown whether the thermal stability of deep-sea DHFRs is related to the environmental temperature of the organisms. Further detailed studies of the thermal and pressure denaturation of deep-sea enzymes are necessary, because the effects of pressure and temperature on protein structures are nonadditive, as typically shown by the elliptic P – T diagram [79,119–121].

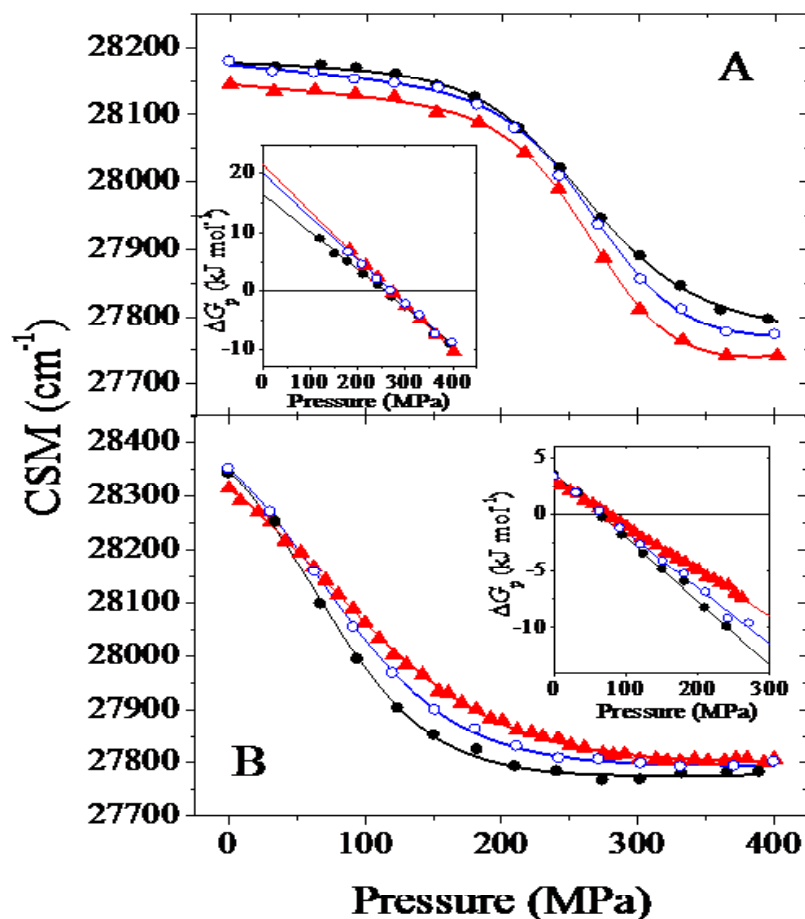


Figure 8: Pressure dependence of the center of fluorescence spectral mass (CSM) of ecDHFR (A) and mpDHFR (B) at pH 8.0. The temperatures were 15.2°C (black filled circles), 20.4°C (blue open circles), and 27.0°C (red filled triangles) for panel A, and 15.7°C (black filled circles), 20.4°C (blue open circles), and 28.8°C (red filled triangles) for panel B. Solid lines represent the theoretical fits to a two-state unfolding model. The insets show the pressure dependence of the apparent Gibbs free-energy change due to pressure denaturation (ΔG_p). (Reproduced from Ohmae et al. [39].)

3.3. Function of deep-sea DHFRs

The K_m and k_{cat} values at atmospheric pressure for ecDHFR, deep-sea DHFRs, and some atmospheric *Shewanella* DHFRs are listed in **Table 3** [37,38]. The K_m values of all of these deep-sea and *Shewanella* DHFRs are larger than that of ecDHFR, especially for mjDHFR. The k_{cat} values of all of these DHFRs are also larger than that of ecDHFR, resulting in a 1.5- to 2.8-fold increase in k_{cat}/K_m with an exceptionally large decrease (28-fold) for mjDHFR. Increases in K_m and k_{cat} were also observed for NADPH, indicating the decreased affinity to a cofactor as well as a substrate [37,38]. Thus, these deep-sea DHFRs are functionally more active than ecDHFR at atmospheric pressure due to the large turnover overcoming the reduced affinity for the substrate, while mjDHFR is less active due to the large reduction in the substrate-binding ability despite the increased turnover.

The effects of pressure on catalytic function are of grave concern for deep-sea enzymes. **Figure 9** shows the pressure dependence of the activities of ecDHFR and some deep-sea DHFRs [38,39]. The activities of three deep-sea DHFRs (svDHFR, mpDHFR, and sb21DHFR; the last is from obligately piezophilic bacterium *S. benthica* strain DB21MT-2 isolated

from the Mariana Trench at a depth of 10,898 m [122]) increased as the pressure increased up to 50 MPa, and then gradually decreased for higher pressures. However, all of the other DHFRs examined did not exhibit such pressure activation, with their activity decreasing monotonically with pressure. This means that deep-sea DHFRs are not necessarily tolerant against pressure, but that some tolerant mechanisms must be involved in these three DHFRs.

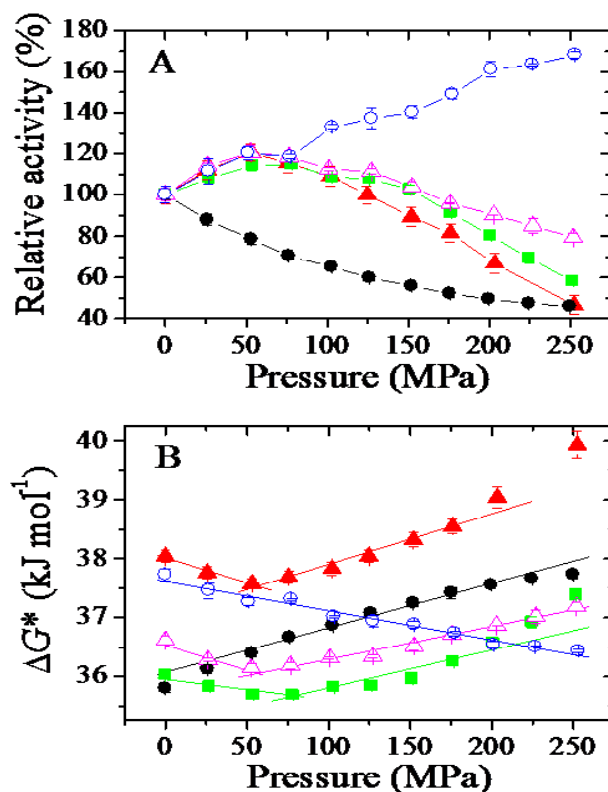


Figure 9: Pressure dependence of the relative activity (A) and activation free energy (B) of deep-sea DHFRs. Three deep-sea DHFRs—mpDHFR (red filled triangles), svDHFR (magenta open triangles), and sb21DHFR (green filled squares)—are compared with wild-type ecDHFR (black filled circles) and its D27E mutant (blue open circles). The experimental temperature was 25.0°C. Lines in panel B indicate linear fits. (Reproduced from Ohmae et al. [40].)

Volumetric data are indispensable for understanding pressure-dependent enzyme reactions. The activation volume (ΔV^*) of a catalytic reaction at a saturated substrate concentration can be estimated from the pressure dependence of the initial velocity (u) of the enzymatic reaction as follows [103]:

$$\Delta V^* = \partial \Delta G^* / \partial P = \partial (-RT \ln(k_{cat})) / \partial P = \partial (-RT \ln(u)) / \partial P \quad (6)$$

where ΔG^* is the activation free energy of the enzymatic reaction and ΔV^* is the volume difference between the transition and ground states in the rate-determining step. As shown in **Figure 2**, the enzymatic reaction of DHFR includes at least five steps: two binding steps involving DHF and NADPH, the chemical oxidation–reduction step (hydride transfer), and two releasing steps involving THF and NADP^+ [5]. The THF-releasing step is the rate-determining step for ecDHFR at neutral pH and atmospheric pressure. Since the two binding steps can hardly be the rate-determining step at saturated concentrations of DHF and NADPH, ΔV^* would mainly arise from the hydride transfer and the two releasing steps.

The ΔV^* values for the deep-sea and homologous DHFRs are listed in **Table 4**. Three DHFRs (ecDHFR, mjDHFR, and ppr9DHFR) whose activities decreased monotonically with pressure show positive ΔV^* values over the pressure range examined. However, as expected from the inversion in the pressure–activity profile (**Figure 9**), other DHFRs show clearly different ΔV^* values below and above a given pressure (25–125 MPa): ΔV^* changes from negative to positive values at around 50 MPa for svDHFR, mpDHFR, and sb21DHFR. The ΔV^* values for any DHFRs are considerably smaller than the volume change due to pressure denaturation (ΔV°), suggesting that ΔV^* would result from local changes in cavities and hydration around the active site. The positive ΔV^* value may be attributed to dehydration induced by the conformational closing of the transition state upon releasing the product or cofactor, since the hydride transfer step (if it is the rate-determining step) would contribute negatively to ΔV^* through hydration of partial charges or condensation of the hydrated water in the transition state [123,124]. The ΔV^* values in high-pressure regions, which were 5.6, 6.5, and 8.6 $\text{cm}^3 \text{mol}^{-1}$ for svDHFR, sb21DHFR, and mpDHFR, respectively, were comparable to that of ecDHFR (7.5 $\text{cm}^3 \text{mol}^{-1}$), suggesting that the rate-determining step of these three DHFRs in high-pressure regions is the release of product as well as ecDHFR. Negative ΔV^* values in a low-pressure region would be possible if the rate-determining step changes to the hydride transfer step and/or if the transition state has the open conformation, because both events could accompany the increase in hydration of the transition state.

These interpretations for the ΔV^* values are clearly oversimplified, and so a more-detailed analysis of the pressure effects on each reaction step is necessary for understanding the pressure-adaptation mechanism of deep-sea DHFRs. However, it is apparent that structural flexibility involving modified cavities and hydration participates in the structural and functional adaptation of deep-sea DHFRs to high-pressure environments.

Table 4: Activation volumes at 25°C and pH 7.0 for the enzymatic reaction of DHFRs obtained from bacteria living in deep-sea and atmospheric-pressure conditions ^a.

DHFR	ΔV^* (cm ³ mol ⁻¹)	
ecDFHR (wild type)	7.5±0.2 (0.1–250 MPa)	
ecDHFR (D27E mutant)	−4.8±0.1 (0.1–250 MPa)	
sb21DHFR	−3.5±0.6 (0.1–75 MPa)	6.5±0.1 (75–250 MPa)
sb6705DHFR	2.0±0.1 (0.1–25 MPa)	29.0±0.3 (25–250 MPa)
sfDHFR	14.0±0.1 (0.1–125 MPa)	30.5±0.2 (125–250 MPa)
soDHFR	4.1±1.4 (0.1–50 MPa)	13.1±0.2 (50–250 MPa)
spDHFR	11.5±0.2 (0.1–125 MPa)	23.3±1.0 (125–250 MPa)
svDHFR	−8.6±1.9 (0.1–50 MPa)	5.6±0.1 (50–250 MPa)
mjDHFR	38.7±0.3 (0.1–250 MPa)	
mpDHFR	−8.6±2.5 (0.1–50 MPa)	8.6±0.9 (50–250 MPa)
myDHFR	1.7±0.6 (0.1–75 MPa)	16.5±0.6 (75–250 MPa)
ppr9DHFR	13.8±0.4 (0.1–250 MPa)	

^a Values in parentheses indicate the pressure range used for the calculation. Taken from Murakami et al. [37,38] and Ohmae et al. [39,134].

3.4. Adaptation mechanisms to deep-sea environments

To understand the adaptation of microorganisms to high-pressure environments, numerous deep-sea piezophilic microorganisms have been isolated and studied over the past 20 years [125,126], focusing on their biodiversity [127,128], pressure-regulated gene expression [129, 130], and genome sequences [131,132]. However, only a few studies regarding protein adaptation to the deep sea have been reported [133–138], and the molecular mechanisms underlying how deep-sea enzymes adapt to high-pressure and other extreme environments remain unclear.

The above-mentioned comparative studies of the stability and function of DHFRs from several deep-sea bacteria and atmospheric-pressure species revealed that three deep-sea DHFRs (svDHFR, mpDHFR, and sb21DHFR) exhibited optimal enzyme activity at approximately 50 MPa. However, pressure decreased the activities of other deep-sea DHFRs such as ppr9DHFR, mjDHFR, and sb6705DHFR (from *S. benthica* strain DB6705). On the other hand, soDHFR from *S. oneidensis* strain MR-1 (isolated from Oneida Lake in the USA [139]) clearly showed pressure tolerance in enzymatic activity up to about 100 MPa [38] despite it being an atmospheric-pressure enzyme. These diverse findings indicate that the activity-optimal pressure of DHFRs is not necessarily correlated with the habitat pressure of the parent bacteria.

According to the taxonomic determination of the isolated deep-sea microorganisms performed on the basis of 5S and 16S ribosomal DNA sequences, approximately half of them

are archaea while others are various kinds of bacteria, but all piezophilic bacteria included in the Gamma-proteobacteria subgroup belong to only five genera: *Shewanella*, *Moritella*, *Psychromonas*, *Photobacterium*, and *Colwellia* [130,140]. Since these five genera also comprise species living in atmospheric-pressure environments, these deep-sea bacteria would have adapted to deep-sea conditions (i.e., high pressure and low temperature) after their genera differentiated in atmospheric-pressure environments. Thus, the high-pressure adaptation mechanism of deep-sea DHFRs would be complicated by evolutionary events.

We recently found that the pressure-dependent activity of ecDHFR was inverted by replacing active-site residue Asp27 with glutamic acid: the activity increased with pressure up to 250 MPa, with a negative ΔV^* (**Figure 9**) [134]. This result is particularly interesting because both amino acids are selected as the active-site residue in deep-sea DHFRs depending on their genera (**Figure 7**). Furthermore, it has been recently found that only a single amino acid substitution dramatically affects the pressure adaptation of a deep-sea enzyme. IPMDH from the extreme piezophile *S. benthica* DB21MT-2 (sbIPMDH) was more pressure-tolerant than that from the atmospheric-pressure-adapted *S. oneidensis* (soIPMDH) despite only a single amino acid differing at the backside of the active center: Ser266 in soIPMDH and Ala266 in sbIPMDH [138]. X-ray structural analyses of soIPMDH indicated that three water molecules penetrated into the cleft around Ser266 under high-pressure conditions so as to reduce the flexibility of the wild-type enzyme, while no water molecule was observed in the Ala266 mutant of soIPMDH that exhibits pressure-tolerant activity similar to that of sbIPMDH [138]. This is the first finding that a single amino acid substitution can play an important role in the pressure adaptation of deep-sea enzymes. This illustrates that mutation studies of deep-sea DHFRs would be fruitful for understanding their pressure-adaptation mechanisms.

4. Concluding Remarks

Structural flexibility is essential for enzyme function. Numerous experimental data and computer simulations have revealed the significant contributions of distal residues to the structural dynamics and catalytic mechanism of ecDHFR. The loop-mutation studies of ecDHFR have demonstrated that local structural changes in flexible loops play substantial roles in the stability, flexibility, and catalytic function of this enzyme *via* modified internal cavities—these loops have not previously been recognized as dynamically and functionally significant. The nonadditive effects of double mutations demonstrate that the motional and energetic coupling between the loops in distant positions is propagated to the active site *via* movement of the Met20 loop. However, a detailed context for the role of dynamics in function remains mysterious because of the complicated motional hierarchy or allosteric effect of protein structure. Further experimental and theoretical studies of distal loop mutants will expand our understanding of the roles of structural flexibility in maintaining the stability and activity of this protein.

In contrast to ecDHFR, deep-sea DHFRs showed significantly different pressure effects on the stability and function, as typically detected in the inversed pressure–activity profile. This also constitutes evidence for the important contribution of internal cavities to structural flexibility. Further comparative studies of DHFRs from various deep-sea bacteria should yield new information to facilitate the understanding of the role of structural flexibility in function and pressure adaptation in relation to molecular evolution. Such information will also be useful for identifying strategies for drug design relevant to DHFR.

5. Acknowledgements

The loop-mutation study of ecDHFR was initiated using the overexpression plasmid that was kindly provided by Dr. Masahiro Iwakura (National Institute of Advanced Industrial Science and Technology). Deep-sea DHFRs were cloned from genomic DNA of the deep-sea bacteria provided by Dr. Chiaki Kato (Japan Agency for Marine-Earth Science and Technology). We thank all collaborators for their helpful discussions and experimental contributions.

6. References

1. Liu CT, Hanojan P, French JB, Pringle TH, Hammes-Schiffer S, Benkovic SJ. Functional significance of evolving protein sequence in dihydrofolate reductase from bacteria to humans. *Proc. Natl. Acad. Sci. USA* 2013; 110: 10159–10164.
2. Francis K, Stojkovic V, Kohen A. Preservation of protein dynamics in dihydrofolate reductase evolution. *J. Biol. Chem.* 2013; 288: 35961–35968.
3. Klinman JP, Kohen A. Evolutionary aspects of enzyme dynamics. *J. Biol. Chem.* 2014; 289: 30205–30212.
4. Masterson JE, Schwartz SD. Evolution alters the enzymatic reaction coordinate of dihydrofolate reductase. *J. Phys. Chem. B.* 2015; 119: 989–996.
5. Fierke CA, Johnson KA, Benkovic SJ. Construction and evaluation of the kinetic scheme associated with dihydrofolate reductase from *Escherichia coli*. *Biochemistry* 1987; 26: 4085–4092.
6. Miller GP, Benkovic SJ. Stretching exercises–flexibility in dihydrofolate reductase catalysis. *Chem. Biol.* 1998; 5: R105–R113.
7. Rajagopalan PT, Benkovic SJ. Preorganization and protein dynamics in enzyme catalysis. *Chem. Rec.* 2002; 2: 24–36.
8. Sawaya MR, Kraut J. Loop and subdomain movements in the mechanism of *Escherichia coli* dihydrofolate reductase: crystallographic evidence. *Biochemistry* 1997; 36: 586–603.
9. Mayer RJ, Chen JT, Taira K, Fierke CA, Benkovic SJ. Importance of a hydrophobic residue in binding and catalysis by dihydrofolate reductase. *Proc. Natl. Acad. Sci. USA* 1986; 83: 7718–7720.
10. Chen JT, Taira K, Tu CP, Benkovic SJ. Probing the functional role of phenylalanine-31 of *Escherichia coli* dihydrofolate reductase by site-directed mutagenesis. *Biochemistry* 1987; 26: 4093–4100.
11. Fierke CA, Benkovic SJ. Probing the functional role of threonine-113 of *Escherichia coli* dihydrofolate reductase for its effect on turnover efficiency, catalysis, and binding. *Biochemistry* 1989; 28: 478–486.

12. Adams JA, Fierke CA, Benkovic SJ. The function of amino acid residues contacting the nicotinamide ring of NADPH in dihydrofolate reductase from *Escherichia coli*. *Biochemistry* 1991; 30: 11046–11054.
13. Warren MS, Brown KA, Farnum MF, Howell EE, Kraut J. Investigation of the functional role of tryptophan-22 in *Escherichia coli* dihydrofolate reductase by site-directed mutagenesis. *Biochemistry* 1991; 30: 11092–11103.
14. David CL, Howell EE, Farnum MF, Villafranca JE, Oatley SJ, Kraut J. Structure and function of alternative proton-relay mutants of dihydrofolate reductase. *Biochemistry* 1992; 31: 9813–9822.
15. Ahrweiler PM, Frieden C. Effects of point mutations in a hinge region on the stability, folding, and enzymatic activity of *Escherichia coli* dihydrofolate reductase. *Biochemistry* 1991; 30: 7801–7809.
16. Farnum MF, Magde D, Howell EE, Hirai JT, Warren MS, Grimsley JK, Kraut J. Analysis of hydride transfer and cofactor fluorescence decay in mutants of dihydrofolate reductase: possible evidence for participation of enzyme molecular motions in catalysis. *Biochemistry* 1991; 30: 11567–11579.
17. Rajagopalan PT, Lutz S, Benkovic SJ. Coupling interactions of distal residues enhance dihydrofolate reductase catalysis: mutational effects on hydride transfer rates. *Biochemistry* 2002; 41: 12618–12628.
18. Radkiewicz JL, Brooks CL 3rd. Protein dynamics in enzymatic catalysis: exploration of dihydrofolate reductase. *J. Am. Chem. Soc.* 2000; 122: 225–231.
19. Dams T, Auerbach G, Bader G, Jacob U, Ploom T, Huber R, Jaenicke R. The crystal structure of dihydrofolate reductase from *Thermotoga maritima*: molecular features of thermostability. *J. Mol. Biol.* 2000; 297: 659–672.
20. Loveridge EJ, Rodriguez RJ, Swanwick RS, Allemann RK. Effect of dimerization on the stability and catalytic activity of dihydrofolate reductase from the hyperthermophile *Thermotoga maritima*. *Biochemistry* 2009; 48: 5922–5933.
21. Loveridge EJ, Allemann RK. The temperature dependence of the kinetic isotope effects of dihydrofolate reductase from *Thermotoga maritima* is influenced by intersubunit interactions. *Biochemistry* 2010; 49: 5390–5396.
22. Xu Y, Feller G, Gerday C, Gransdorff N. *Moritella* cold-active dihydrofolate reductase: are there natural limits to optimization of catalytic efficiency at low temperature? *J. Bacteriol.* 2003; 185: 5519–5526.
23. Hay S, Evans RM, Levy C, Loveridge EJ, Wang X, Leys D, Allemann RK, Scrutton NS. Are the catalytic properties of enzymes from piezophilic organisms pressure adapted? *Chembiochem* 2009; 10: 2348–2353.
24. Evans RM, Behiry EM, Tey LH, Guo J, Loveridge EJ, Allemann RK. Catalysis by dihydrofolate reductase from the psychropiezophile *Moritella profunda*. *Chembiochem* 2010; 11: 2010–2017.
25. Pieper U, Kapadia G, Mevarech M, Herzberg O. Structural features of halophilicity derived from the crystal structure of dihydrofolate reductase from the Dead Sea halophilic archaeon, *Haloferax volcanii*. *Structure* 1998; 6: 75–88.
26. Wright DB, Banks DD, Lohman JR, Hilsenbeck JL, Gloss LM. The effect of salts on the activity and stability of *Escherichia coli* and *Haloferax volcanii* dihydrofolate reductases. *J. Mol. Biol.* 2002; 323: 327–344.
27. Boroujerdi AF, Young JK. NMR-derived folate-bound structure of dihydrofolate reductase 1 from the halophile *Haloferax volcanii*. *Biopolymers* 2009; 91: 140–144.
28. Miyashita Y, Ohmae E, Nakasone K, Katayanagi K. Effects of salt on the structure, stability, and function of a halophilic dihydrofolate reductase from a hyperhalophilic archaeon, *Haloarcula japonica* strain TR-1. *Extremophiles* 2015; 19: 479–493.
29. Miyashita Y, Ohmae E, Ikura T, Nakasone K, Katayanagi K. Halophilic mechanism of the enzymatic function of a moderately halophilic dihydrofolate reductase from *Haloarcula japonica* strain TR-1. *Extremophiles* 2017; 21: 591–602.
30. Redecke L, Brehm MA, Bredehorst R. Cloning and characterization of dihydrofolate reductase from a facultative

alkaliphilic and halotolerant bacillus strain. *Extremophiles* 2007; 11: 75–83.

31. Gekko K, Yamagami K, Kunori Y, Ichihara S, Kodama M, Iwakura M. Effects of point mutations in a flexible loop on the stability and enzymatic function of *Escherichia coli* dihydrofolate reductase. *J. Biochem.* 1993; 113: 74–80.
32. Gekko K, Kunori Y, Takeuchi H, Ichihara S, Kodama M. Point mutations at glycine-121 of *Escherichia coli* dihydrofolate reductase: important roles of a flexible loop in the stability and function. *J. Biochem.* 1994; 116: 34–41.
33. Ohmae E, Iriyama K, Ichihara S, Gekko K. Effects of point mutation at a flexible loop glycine-67 of *Escherichia coli* dihydrofolate reductase on its stability and function. *J. Biochem.* 1996; 119: 703–710.
34. Ohmae E, Ishimura K, Iwakura M, Gekko K. Effects of point mutation at a flexible loop alanine-145 of *Escherichia coli* dihydrofolate reductase on its stability and function. *J. Biochem.* 1998; 123: 839–846.
35. Ohmae E, Iriyama K, Ichihara S, Gekko K. Nonadditive effects of double mutations at the flexible loops, glycine-67 and glycine-121, of *Escherichia coli* dihydrofolate reductase on its stability and function. *J. Biochem.* 1998; 123: 33–41.
36. Gekko K, Ohmae E. Analysis of loop function of dihydrofolate reductase. *Seibutsu Butsuri* 2004; 44: 70–74.
37. Murakami C, Ohmae E, Tate S, Gekko K, Nakasone K, Kato C. Cloning and characterization of dihydrofolate reductases from deep-sea bacteria. *J. Biochem.* 2010; 147: 591–599.
38. Murakami C, Ohmae E, Tate S, Gekko K, Nakasone K, Kato C. Comparative study on dihydrofolate reductases from *Shewanella* species living in deep-sea and ambient atmospheric-pressure environments. *Extremophiles* 2011; 15: 165–175.
39. Ohmae E, Murakami C, Tate S, Gekko K, Hata K, Akasaka K, Kato C. Pressure dependence of activity and stability of dihydrofolate reductases of the deep-sea bacterium *Moritella profunda* and *Escherichia coli*. *Biochim. Biophys. Acta* 2012; 1824: 511–519.
40. Ohmae E, Gekko K, Kato C. Environmental adaptation of dihydrofolate reductase from deep-sea bacteria. In *High Pressure Bioscience* (Akasaka K, Matsuki H, eds.), Springer, New York, 2015; pp. 423–442.
41. Schnell JR, Dyson HJ, Wright PE. Structure, dynamics, and catalytic function of dihydrofolate reductase. *Annu. Rev. Biophys. Biomol. Struct.* 2004; 33: 119–140.
42. Hammes-Schiffer S, Benkovic SJ. Relating protein motion to catalysis. *Annu. Rev. Biochem.* 2006; 75: 519–541.
43. Hammes GG, Benkovic SJ, Hammes-Schiffer S. Flexibility, diversity, and cooperativity: pillars of enzyme catalysis. *Biochemistry* 2011; 50: 10422–10430.
44. Arora K, Brooks CL 3rd. Multiple intermediates, diverse conformations, and cooperative conformational changes underlie the catalytic hydride transfer reaction of dihydrofolate reductase. *Top Curr. Chem.* 2013; 337: 165–187.
45. Kohen A. Dihydrofolate reductase as a model for studies of enzyme dynamics and catalysis. *F1000Res.* 2015; 4(F1000 Faculty Rev.): 1464.
46. Luk LYP, Loveridge EJ, Allemann RK. Protein motions and dynamic effects in enzyme catalysis. *Phys. Chem. Chem. Phys.* 2015; 17: 30817–30827.
47. Bolin JT, Filman DJ, Matthews DA, Hamlin RC, Kraut J. Crystal structures of *Escherichia coli* and *Lactobacillus casei* dihydrofolate reductase refined at 1.7 Å resolution. I. General features and binding of methotrexate. *J. Biol. Chem.* 1982; 257: 13650–13662.
48. Epstein DM, Benkovic SJ, Wright PE. Dynamics of the dihydrofolate reductase–folate complex: catalytic sites and regions known to undergo conformational change exhibit diverse dynamical features. *Biochemistry* 1995; 34: 11037–11048.

49. Benkovic SJ, Fierke CA, Naylor AM. Insights into enzyme function from studies on mutants of dihydrofolate reductase. *Science* 1988; 239: 1105–1110.
50. Cameron CE, Benkovic SJ. Evidence for a functional role of the dynamics of glycine-121 of *Escherichia coli* dihydrofolate reductase obtained from kinetic analysis of a site-directed mutant. *Biochemistry* 1997; 36: 15792–15800.
51. Lau EY, Gerig JT. Effects of fluorine substitution on the structure and dynamics of complexes of dihydrofolate reductase (*Escherichia coli*). *Biophys. J.* 1997; 73: 1579–1592.
52. Miller GP, Wahnon DC, Benkovic SJ. Interloop contacts modulate ligand cycling during catalysis by *Escherichia coli* dihydrofolate reductase. *Biochemistry* 2001; 40: 867–875.
53. Osborne MJ, Schnell J, Benkovic SJ, Dyson HJ, Wright PE. Backbone dynamics in dihydrofolate reductase complexes: role of loop flexibility in the catalytic mechanism. *Biochemistry* 2001; 40: 9846–9859.
54. Rod TH, Radkiewicz JL, Brooks CL 3rd. Correlated motion and the effect of distal mutations in dihydrofolate reductase. *Proc. Natl. Acad. Sci. USA* 2003; 100: 6980–6985.
55. Wong KF, Selzer T, Benkovic SJ, Hammes-Schiffer S. Impact of distal mutations on the network of coupled motions correlated to hydride transfer in dihydrofolate reductase. *Proc. Natl. Acad. Sci. USA* 2005; 102: 6807–6812.
56. Arora K, Brooks CL 3rd. Functionally important conformations of the Met20 loop in dihydrofolate reductase are populated by rapid thermal fluctuations. *J. Am. Chem. Soc.* 2009; 131: 5642–5647.
57. Luo J, Bruice TC. Envisioning the loop movements and rotation of the two subdomains of dihydrofolate reductase by elastic normal mode analysis. *J. Biomol. Struct. Dyn.* 2009; 27: 245–258.
58. Bhabha G, Lee J, Ekiert DC, Gam J, Wilson IA, Dyson HJ, Benkovic SJ, Wright PE. A dynamic knockout reveals that conformational fluctuations influence the chemical step of enzyme catalysis. *Science* 2011; 332: 234–238.
59. Boehr DD, Schnell JR, McElheny D, Bae SH, Duggan BM, Benkovic SJ, Dyson HJ, Wright PE. A distal mutation perturbs dynamic amino acid networks in dihydrofolate reductase. *Biochemistry* 2013; 52: 4605–4619.
60. Singh P, Sen A, Francis K, Kohen A. Extension and limits of the network of coupled motions correlated to hydride transfer in dihydrofolate reductase. *J. Am. Chem. Soc.* 2014; 136: 2575–2582.
61. Francis K, Kohen A. Protein motions and the activation of the CH bond catalyzed by dihydrofolate reductase. *Curr. Opin. Chem. Biol.* 2014; 21: 19–24.
62. Agarwal PK, Billeter SR, Rajagopalan PT, Benkovic SJ, Hammes-Schiffere S. Network of coupled promoting motions in enzyme catalysis. *Proc. Natl. Acad. Sci. USA* 2002; 99: 2794–2799.
63. Mauldin RV, Lee AL. NMR study of the role of M42 in the solution dynamics of *E. coli* dihydrofolate reductase. *Biochemistry* 2010; 49: 1606–1615.
64. Ohmae E, Fukumizu Y, Iwakura M, Gekko K. Effects of mutations at methionine-42 of *Escherichia coli* dihydrofolate reductase on its stability and function: implication of hydrophobic interactions. *J. Biochem.* 2005; 137: 643–652.
65. Shellman JA. Solvent denaturation. *Biopolymers* 1978; 17: 1305–1322.
66. Pace CN. Determination and analysis of urea and guanidine hydrochloride denaturation curves. In *Methods in Enzymology*, Vol. 131 (Hirs CHW, Timasheff SN, eds.), Academic Press, New York, 1985; pp. 267–280.
67. Shortle D. Staphylococcal nuclease: a showcase of m-value effects. *Adv. Protein Chem.* 1995; 46: 217–247.
68. Mildvan AS, Weber DJ, Kuliopulos A. Quantitative interpretations of double mutations of enzymes. *Arch. Biochem. Biophys.* 1992; 294: 327–340.

69. Swanwick RS, Shrimpton PJ, Allemann RK. Pivotal role of Gly 121 in dihydrofolate reductase from *Escherichia coli*: the altered structure of a mutant enzyme may form the basis of its diminished catalytic performance. *Biochemistry* 2004; 43: 4119–4127.
70. Ohmae E, Kurumiya T, Makino S, Gekko K. Acid and thermal unfolding of *Escherichia coli* dihydrofolate reductase. *J. Biochem.* 1996; 120: 946–953.
71. Kuwajima K, Garvey EP, Finn BE, Matthews CR, Sugai S. Transient intermediates in the folding of dihydrofolate reductase as detected by far-ultraviolet circular dichroism spectroscopy. *Biochemistry* 1991; 30: 7693–7703.
72. Horiuchi Y, Ohmae E, Tate S, Gekko K. Coupling effects of distal loops on structural stability and enzymatic activity of *Escherichia coli* dihydrofolate reductase revealed by deletion mutants. *Biochim. Biophys. Acta* 2010; 1804: 846–855.
73. Bystroff C, Kraut J. Crystal structure of unliganded *Escherichia coli* dihydrofolate reductase. Ligand-induced conformational changes and cooperativity in binding. *Biochemistry* 1991; 30: 2227–2239.
74. Falzone CJ, Wright PE, Benkovic SJ. Evidence for two interconverting protein isomers in the methotrexate complex of dihydrofolate reductase from *Escherichia coli*. *Biochemistry* 1991; 30: 2184–2191.
75. Kitahara R, Sareth S, Yamada H, Ohmae E, Gekko K, Akasaka K. High pressure NMR reveals active-site hinge motion of folate-bound *Escherichia coli* dihydrofolate reductase. *Biochemistry* 2000; 39: 12789–12795.
76. Gekko K, Tamura Y, Ohmae E, Hayashi H, Kagamiyama H, Ueno H. A large compressibility change of protein induced by a single amino acid substitution. *Protein Sci.* 1996; 5: 542–545.
77. Gekko K, Kamiyama T, Ohmae E, Katayanagi K. Single amino acid substitutions in flexible loops can induce large compressibility changes in dihydrofolate reductase. *J. Biochem.* 2000; 128: 21–27.
78. Kamiyama T, Gekko K. Effects of ligand binding on the flexibility of dihydrofolate reductase as revealed by compressibility. *Biochim. Biophys. Acta* 2000; 1478: 257–266.
79. Gekko K. Volume and compressibility of proteins. In *High Pressure Bioscience* (Akasaka K, Matsuki H, eds.), Springer, New York, 2015; pp. 75–108.
80. Cooper A. Thermodynamic fluctuations in protein molecules. *Proc. Natl. Acad. Sci. USA* 1976; 73: 2740–2741.
81. Gekko K, Hasegawa Y. Compressibility–structure relationship of globular proteins. *Biochemistry* 1986; 25: 6563–6571.
82. Englander SW, Kallenbach NR. Hydrogen exchange and structural dynamics of proteins and nucleic acids. *Q. Rev. Biophys.* 1983; 16: 521–655.
83. Englander JJ, Del Mar C, Li W, Englander SW, Kim JS, Stranz DD, Hamuro Y, Woods VL Jr. Protein structure change studied by hydrogen-deuterium exchange, functional labeling, and mass spectrometry. *Proc. Natl. Acad. Sci. USA* 2003; 100: 7057–7062.
84. Nakanishi M, Tsuboi M. Structure and fluctuation of a *Streptomyces* subtilisin inhibitor. *Biochim. Biophys. Acta* 1976; 434: 365–376.
85. Akasaka K, Inoue T, Hatano H, Woodward CK. Hydrogen exchange kinetics of core peptide protons in *Streptomyces* subtilisin inhibitor. *Biochemistry* 1985; 24: 2973–2979.
86. Zhang Z, Smith DL. Determination of amide hydrogen exchange by mass spectrometry: a new tool for protein structure elucidation. *Protein Sci.* 1993; 2: 522–531.
87. Powell KD, Wales TE, Fitzgerald MC. Thermodynamic stability measurements on multimeric proteins using a new H/D exchange- and matrix-assisted laser desorption/ionization (MALDI) mass spectrometry-based method. *Protein Sci.*

2002; 11: 841–851.

88. Yamamoto T, Izumi S, Gekko K. Mass spectrometry on segment-specific hydrogen exchange of dihydrofolate reductase. *J. Biochem.* 2004; 135: 17–24.

89. Yamamoto T, Izumi S, Ohmae E, Gekko K. Mass spectrometry of hydrogen/deuterium exchange of *Escherichia coli* dihydrofolate reductase: effects of loop mutations. *J. Biochem.* 2004; 135: 487–494.

90. Miller GP, Benkovic SJ. Deletion of a highly motional residue affects formation of the Michaelis complex for *Escherichia coli* dihydrofolate reductase. *Biochemistry* 1998; 37: 6327–6335.

91. Wang L, Tharp S, Selzer T, Benkovic SJ, Kohen A. Effects of a distal mutation on active site chemistry. *Biochemistry* 2006; 45: 1383–1392.

92. Wang L, Goodey NM, Benkovic SJ, Kohen A. The role of enzymatics and tunneling in catalyzing hydride transfer: studies of distal mutants of dihydrofolate reductase. *Phil. Trans. Soc. London, Ser. B* 2006; 361: 1307–1315.

93. Mauldin RV, Sapienza PJ, Petit CM, Lee AL. Structure and dynamics of the G121V dihydrofolate reductase mutant: lessons from a transition-state inhibitor complex. *PLoS One* 2012; 7: e33252.

94. Tan XH, Huang SM, Ratnam M, Thompson PD, Freisheim JH. The importance of loop region residues 40–46 in human dihydrofolate reductase as revealed by site-directed mutagenesis. *J. Biol. Chem.* 1990; 265: 8027–8032.

95. Yamamoto T, Izumi S, Gekko K. Mass spectrometry on hydrogen/deuterium exchange of dihydrofolate reductase: effects of ligand binding. *J. Biochem.* 2004; 135: 663–671.

96. Balog E, Becker T, Oetl M, Lechner R, Daniel R, Finney J, Smith JC. Direct determination of vibrational density of states change on ligand binding to a protein. *Phys. Rev. Lett.* 2004; 93: 028103.

97. Balog E, Perahia D, Smith JC, Merzel F. Vibrational softening of a protein on ligand binding. *J. Phys. Chem. B* 2011; 115: 6811–6817.

98. Iwakura M, Maki K, Takahashi H, Takenawa T, Yokota A, Katayanagi K, Kamiyama T, Gekko K. Evolutional design of a hyperactive cysteine- and methionine-free mutant of *Escherichia coli* dihydrofolate reductase. *J. Biol. Chem.* 2006; 281: 13234–13246.

99. Gekko K, Obu M, Li J, Lee JC. A linear correlation between the energetics of allosteric communication and protein flexibility in the *Escherichia coli* cyclic AMP receptor protein revealed by mutation-induced changes in compressibility and amide hydrogen-deuterium exchange. *Biochemistry* 2004; 43: 3844–3852.

100. Bartlett DH, Kato C, Horikoshi K. High pressure influences on gene and protein expression. *Res. Microbiol.* 1995; 146: 697–706.

101. Abe F, Kato C, Horikoshi K. Pressure-regulated metabolism in microorganisms. *Trends Microbiol.* 1999; 7: 447–453.

102. Nakasone K, Ikegami A, Kawano H, Kato C, Usami R, Horikoshi K. Transcriptional regulation under pressure conditions by RNA polymerase sigma54 factor with a two-component regulatory system in *Shewanella violacea*. *Extremophiles* 2002; 6: 89–95.

103. Ohmae E, Tatsuta M, Abe F, Kato C, Tanaka N, Kunugi S, Gekko K. Effects of pressure on enzyme function of *Escherichia coli* dihydrofolate reductase. *Biochim. Biophys. Acta* 2008; 1784: 1115–1121.

104. Kato C, Sato T, Horikoshi K. Isolation and properties of barophilic and barotolerant bacteria from deep-sea mud samples. *Biodivers. Conserv.* 1995; 4: 1–9.

105. Nogi Y, Kato C, Horikoshi K. Taxonomic studies of deep-sea barophilic *Shewanella* strains and description of *Shewanella violacea* sp. nov. *Arch. Microbiol.* 1998; 170: 331–338.

106. Ohmae E, Kubota K, Nakasone K, Kato C, Gekko K. Pressure-dependent activity of dihydrofolate reductase from a deep-sea bacterium *Shewanella violacea* strain DSS12. *Chem. Lett.* 2004; 33: 798–799.
107. Nagae T, Kato C, Watanabe N. Structural analysis of 3-isopropylmalate dehydrogenase from the obligate piezophile *Shewanella benthica* DB21MT-2 and the nonpiezophile *Shewanella oneidensis* MR-1. *Acta Crystallogr. F* 2012 ; 68: 265–268.
108. De Vos D, Xu Y, Hulpiau P, Vergauwen B, Van Beeumen JJ. Structural investigation of cold activity and regulation of aspartate carbamoyltransferase from the extreme psychrophilic bacterium *Moritella profunda*. *J. Mol. Biol.* 2007; 365: 379–395.
109. Shirai T, Hung VS, Morinaka K, Kobayashi T, Ito S. Crystal structure of GH13 α -glucosidase GSJ from one of the deepest sea bacteria. *Proteins* 2008; 73: 126–133.
110. Teh AH, Kanamasa S, Kajiwara S, Kumasaka T. Structure of Cu/Zn superoxide dismutase from the heavy-metal-tolerant yeast *Cryptococcus liquifaciens* strain N6. *Biochem. Biophys. Res. Com.* 2008; 374: 475–478.
111. Shin DS, DiDonato M, Barondeau DP, Hura GL, Hitomi C, Berglund JA, Getzoff ED, et al. Superoxide dismutase from the eukaryotic thermophile *Alvinella pompejana*: structures, stability, mechanism, and insights into amyotrophic lateral sclerosis. *J. Mol. Biol.* 2009; 385: 1534–1555.
112. Purcarea C, Hervé G, Ladjimi MM, Cunin R. Aspartate transcarbamylase from the deep-sea hyperthermophilic archaeon *Pyrococcus abyssi*: genetic organization, structure, and expression in *Escherichia coli*. *J. Bacteriol.* 1997; 179: 4143–4157.
113. Saito R, Kato C, Nakayama A. Amino acid substitutions in malate dehydrogenases of piezophilic bacteria isolated from intestinal contents of deep-sea fishes retrieved from the abyssal zone. *J. Gen. Appl. Microbiol.* 2006; 52: 9–19.
114. Brindley AA, Pickersgill RW, Partridge JC, Dunstan DJ, Hunt DM, Warren MJ. Enzyme sequence and its relationship to hyperbaric stability of artificial and natural fish lactate dehydrogenases. *PLoS One* 2008; 3: e2042.
115. Xie BB, Bian F, Chen XL, He HL, Guo J, Gao X, Zeng YX, et al. Cold adaptation of zinc metalloproteases in the thermolysin family from deep sea and Arctic sea ice bacteria revealed by catalytic and structural properties and molecular dynamics: new insights into relationship between conformational flexibility and hydrogen bonding. *J. Biol. Chem.* 2009; 284: 9257–9269.
116. Oefner C, D’Arcy A, Winkler FK. Crystal structure of human dihydrofolate reductase complexed with folate. *Eur. J. Biochem.* 1988; 174: 377–385.
117. Stammers DK, Champness JN, Beddell CR, Dann JG, Eliopoulos E, Geddes AJ, Ogg D, North AC. The structure of mouse L1210 dihydrofolate reductase–drug complexes and the construction of a model of human enzyme. *FEBS Lett.* 1987; 218: 178–184.
118. Kamiyama T, Ohmae E, Gekko K. Large flexibility of dihydrofolate reductase as revealed by temperature effects on the volume and compressibility. *Chem. Lett.* 1999; 28: 507–508.
119. Brandts JF, Oliveira RJ, Westort C. Thermodynamics of protein denaturation. Effect of pressure on the denaturation of ribonuclease A. *Biochemistry* 1970; 9: 1038–1047.
120. Hawley SA. Reversible pressure-temperature denaturation of chymotrypsinogen. *Biochemistry* 1971; 10: 2436–2442.
121. Zipp A, Kauzmann W. Pressure denaturation of metmyoglobin. *Biochemistry* 1973; 12: 4217–4228.
122. Kato C, Li L, Nogi Y, Nakamura Y, Tamaoka J, Horikoshi K. Extremely barophilic bacteria isolated from the Mariana Trench, Challenger Deep, at a depth of 11,000 meters. *Appl. Environ. Microbiol.* 1998; 64: 1510–1513.

123. Northrop DB, Cho YK Effects of pressure on deuterium isotope effects of yeast alcohol dehydrogenase: evidence for mechanical models of catalysis. *Biochemistry* 2000; 39: 2406–2412.
124. Quirk DJ, Northrop DB. Effect of pressure on deuterium isotope effects of formate dehydrogenase. *Biochemistry* 2001; 40: 847–851.
125. Prieur D, Bartlett D, Kato C, Oger Ph, Jebbar M. Piezophilic prokaryotes. In *Comparative High Pressure Biology* (Sébert P, ed.), Science Publishers, Enfield, NH, 2010; pp. 285–322.
126. Kato C. Microbiology of piezophiles in deep-sea environments. In *Extremophiles: Microbiology and Biotechnology* (Anitori RP, ed.), Caister Academic Press, Norfolk, UK, 2012; pp. 233–263.
127. Fang J, Kato C. Deep-sea piezophilic bacteria: geomicrobiology and biotechnology. In *Geomicrobiology: Biodiversity and Biotechnology* (Jain SK, Khan AA, Rai MK, eds.), CRC Press, Boca Raton, 2010; pp. 47–77.
128. Kato C. Cultivation methods for piezophiles. In *Extremophiles Handbook* (Horikoshi K, Antranikian G, Bull A, Robb F, Stetter K, eds.), Springer, Tokyo, 2011; pp. 719–726.
129. Bartlett DH. Pressure effects on in vivo microbial processes. *Biochim. Biophys. Acta* 2002; 1595: 367–381.
130. Kato C. Distribution of piezophiles. In *Extremophiles Handbook* (Horikoshi K, Antranikian G, Bull A, Robb F, Stetter K, eds.), Springer, Tokyo, 2011; pp. 643–655.
131. Vezzi A, Campanaro S, D'Angelo M, Simonato F, Vitulo N, Lauro FM, Cestaro A, et al. Life at depth: *Photobacterium profundum* genome sequence and expression analysis. *Science* 2005; 307: 1459–1461.
132. Aono E, Baba T, Ara T, Nishi T, Nakamichi T, Inamoto E, Toyonaga H, et al. Complete genome sequence and comparative analysis of *Shewanella violacea*, a psychrophilic and piezophilic bacterium from deep sea floor sediments. *Mol. Biosyst.* 2010; 6: 1216–1226.
133. Yano JK, Poulos TL. New understandings of thermostable and peizostable enzymes. *Curr. Opin. Biotechnol.* 2003; 14: 360–365.
134. Ohmae E, Miyashita Y, Tate S, Gekko K, Kitazawa S, Kitahara R, Kuwajima K. Solvent environments significantly affect the enzymatic function of *Escherichia coli* dihydrofolate reductase: comparison of wild-type protein and active-site mutant D27E. *Biochim. Biophys. Acta* 2013; 1834: 2782–2794.
135. Ohmae E, Miyashita Y, Kato C. Thermodynamic and functional characteristics of deep-sea enzymes revealed by pressure effects. *Extremophiles* 2013; 17: 701–709.
136. Davydov DR, Sineva EV, Davydova NY, Bartlett DH, Halpert JR. CYP261 enzymes from deep sea bacteria: a clue to conformational heterogeneity in cytochromes P450. *Biotechnol. Appl. Biochem.* 2013; 60: 30–40.
137. Troeppner O, Lippert R, Shubina TE, Zahl A, Jux N, Ivanović-Burmazović I. Reverse spin-crossover and high-pressure kinetics of the heme iron center relevant for the operation of heme proteins under deep-sea conditions. *Angew. Chem. Int. Ed. Engl.* 2014; 53: 11452–11457.
138. Hamajima Y, Nagae T, Watanabe N, Ohmae E, Kato-Yamada Y, Kato C. Pressure adaptation of 3-isopropylmalate dehydrogenase from an extremely piezophilic bacterium is attributed to a single amino acid substitution. *Extremophiles* 2016; 20:177–186.
139. Venkateswaran K, Moser DP, Dollhopf ME, Lies DP, Saffarini DA, MacGregor BJ, Ringelberg DB, et al. Polyphasic taxonomy of the genus *Shewanella* and description of *Shewanella oneidensis* sp.nov. *Int. J. Syst. Bacteriol.* 1999; 49: 705–724.
140. Nogi Y. Bacteria in the deep sea: psychropiezophiles. In *Psychrophiles: from Biodiversity to Biotechnology* (Margesin R, Schinner F, Marx JC, Gerday C, eds.), Springer, Berlin, 2008; pp. 73–82.